OPTICAL COMMUNICATIONS BETWEEN UNDERWATER AND ABOVE-SURFACE (SATELLITE) TERMINALS

S. Karp

Naval Electronics Laboratory Center
San Diego, California

1 June 1975

NELC / TD 430

Technical Document 430

OPTICAL SATCOM
NELC/NRL

OPTICAL COMMUNICATIONS BETWEEN UNDERWATER AND ABOVE-SURFACE (SATELLITE) TERMINALS

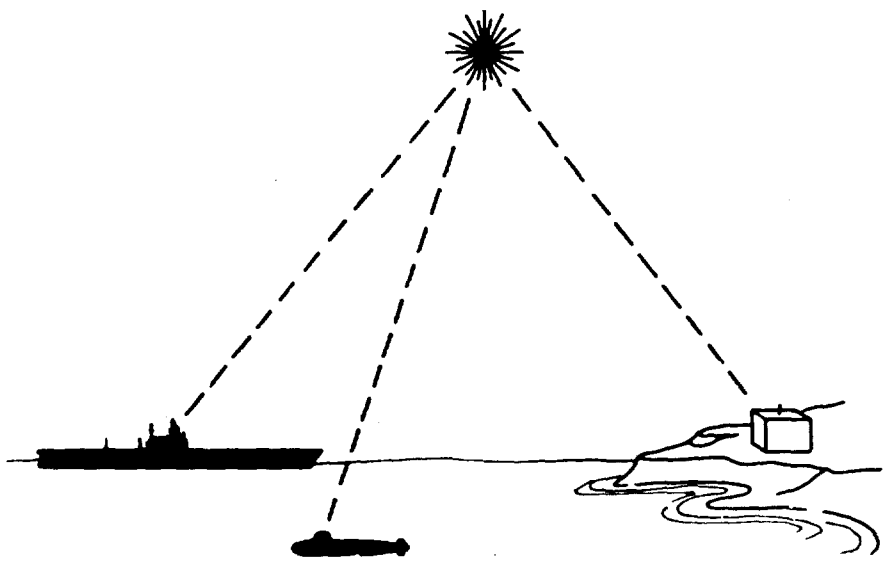

S. Karp

1 June 1975

Prepared for
Office of Naval Research

NAVAL ELECTRONICS LABORATORY CENTER
San Diego, California 92152

UNCLASSIFIED

SECURITY CLASSIFICATION OF THIS PAGE *(When Data Entered)*

REPORT DOCUMENTATION PAGE		READ INSTRUCTIONS BEFORE COMPLETING FORM
1. REPORT NUMBER NELC Technical Document 430 (TD 430)	2. GOVT ACCESSION NO.	3. RECIPIENT'S CATALOG NUMBER
4. TITLE *(and Subtitle)* OPTICAL COMMUNICATIONS BETWEEN UNDERWATER AND ABOVE-SURFACE (SATELLITE) TERMINALS		5. TYPE OF REPORT & PERIOD COVERED 6. PERFORMING ORG. REPORT NUMBER
7. AUTHOR(s) S. Karp		8. CONTRACT OR GRANT NUMBER(s)
9. PERFORMING ORGANIZATION NAME AND ADDRESS Naval Electronics Laboratory Center San Diego, California 92152		10. PROGRAM ELEMENT, PROJECT, TASK AREA & WORK UNIT NUMBERS 60000N, NRL, NIF (NELC J425)
11. CONTROLLING OFFICE NAME AND ADDRESS Office of Naval Research		12. REPORT DATE 1 June 1975 13. NUMBER OF PAGES 44
14. MONITORING AGENCY NAME & ADDRESS*(if different from Controlling Office)*		15. SECURITY CLASS. *(of this report)* Unclassified 15a. DECLASSIFICATION/DOWNGRADING SCHEDULE

16. DISTRIBUTION STATEMENT *(of this Report)*

Approved for public release; distribution is unlimited

17. DISTRIBUTION STATEMENT *(of the abstract entered in Block 20, if different from Report)*

18. SUPPLEMENTARY NOTES

19. KEY WORDS *(Continue on reverse side if necessary and identify by block number)*

Optical communication -- Blue/green
Spacecraft communication -- Terminals
Mathematical models -- Multiple scattering
Subsurface communications -- Terminals
Air/sea interface

20. ABSTRACT *(Continue on reverse side if necessary and identify by block number)*

A multiple scattering model is used and extended to characterize the channel between underwater and airborne (satellite) terminals at optical frequencies. The effects of the air/sea interface are also included with approximate solutions accurate for elevation angles above 45°. The results are presented in terms of a radiance function which is related to the transform of the spatial covariance function (mutual coherence function). The primary losses are shown to be a result of the water absorption coefficient and not the extinction coefficient. The scattering losses can be isolated from the absorption losses and for certain cases, in which the receiver is embedded in the scattering medium, can be completely recovered. New components may be required to

DD FORM 1 JAN 73 1473 EDITION OF 1 NOV 65 IS OBSOLETE
S/N 0102-014-6601

UNCLASSIFIED

SECURITY CLASSIFICATION OF THIS PAGE *(When Data Entered)*

20. ABSTRACT (Continued).

achieve this performance. The effects of ocean roughness are shown to have a minimal effect upon subsurface reception while causing possible beam steering of subsurface transmission. Although substantial losses are experienced, duplex operation can be achieved at modest data rates.

CONTENTS

ACKNOWLEDGMENT

The author would like to acknowledge computational support provided by M. R. Paulson, UHF Technology Division, and P. A. Singer, Monitoring and Switching Technology Division, during the preparation of this manuscript.

INTRODUCTION

The acceptance of optical communications for use in operational systems has been severely hampered by our inability to adequately compensate for channel effects induced by the environment. Consequently, most if not all of the projected system gains are quickly nullified when rudimentary measures of system margin are added to the link budgets to account for these effects. It is, therefore, extremely important that environmental effects be accurately accounted for, and systems designed to best exploit these channels in a most advantageous manner. The most difficult channel that the optical communications engineer has to deal with is the multiple scattering channel. Such a channel exists in propagating through clouds, fog, water, etc. [ref 1-3]. In this document we will extend the model, which has been independently developed by Heggestad [4] and Arnush [5] for multiple scattering media, and apply it to compute the effects we would encounter while traversing a satellite to underwater channel. In doing so, we will try to validate the use and interpretation of the model by applying it to experimental data.

In its most general form, the problem of optical communications between a satellite and a submerged platform can be described as: (1) a problem in communications from a platform in a nonscattering, nondispersive environment, through a random surface, and into a medium with a different index, which is multiple scattering, absorbing, and dispersive; and, conversely, (2) a problem in communications from a platform in a multiple scattering, absorbing, and dispersive medium, through a random surface, and into a medium with a different index which is nonscattering and nondispersive. These two problems are nonreciprocal. Thus, it is necessary to decompose them into their fundamental elements and to individually identify and characterize the contributing factors. To this end, this discussion is divided into four parts. The first part (the underwater channel) involves the actual propagation effects encountered while traversing a multiple scattering medium. The three system parameters which can be identified are attenuation, beam spreading, and apparent source size. These in turn are related to the absorption coefficient, the scattering coefficient, and the volume scattering function. The second part (the air/sea interface) addresses the problem of transmitting through a random surface characterized by a slope distribution. The effect on scintillation is discussed in addition to beam pointing and beam broadening. The third and fourth parts address link calculations from the satellite platform to the submerged platform and from the submerged platform to the satellite platform, respectively. It is estimated that the model presented can be verified to within several dB over most operational scenarios envisioned.

---

1. Kennedy, R. S., "Communication through Optical Scattering Channels: An Introduction," Proc IEEE, vol 58, no 10, p 1651-65, 1970
2. Lerner, R. M., and Holland, A. E., "The Optical Scatter Channel," Proc IEEE, vol 58, no 10, p 1547-1563, 1970
3. Bucher, E. A., Lerner, R. M., and Niessen, C. W., "Some Experiments on the Propagation of Light Pulses through Clouds," Proc IEEE, vol 58, no 10, p 1564-67, 1970
4. Heggestad, H. M., "Optical Communication through Multiple Scattering Media," MIT/RLE Technical Report 472, November 1968
5. Arnush, D., "Underwater Light-Beam Propagation in the Small-Angle Scattering Approximation," JOSA, 62, p 1109-1111, 1972

THE UNDERWATER CHANNEL

Over the past 2 decades there has been an interest in understanding the behavior of light while propagating through water. With the advent of the laser this interest intensified within the context of operational equipment. Although there have been numerous measurements [6, 7] and many empirical curves have been derived to fit the data [7], the latter are of limited use for extrapolating system performance. For this document, we will use a model which has been developed independently by two separate authors [4, 5]. While this model is derived for small-angle forward scattering, it appears to be fairly accurate out to ±45° provided the optical thickness is neither too large nor too small. Fortunately, the range of validity is within the operational ranges envisioned. The model describes the radiance transfer within the multiple-scattering region. This region is characterized by three variables.

1. Absorption. The absorption coefficient of the medium, a, is the amount of energy absorbed by the medium per unit length of propagation. This loss is attenuation, and goes directly into heating and other irreversible processes.

2. Scattering function $F(\theta)$. Multiple scattering media are characterized by scattering centers which, in the case of ocean water, appear to be both from plankton and from molecular scattering. The volume scattering function is defined as the secondary radiation pattern created by a plane wave traversing a small enough volume so that only single scattering occurs. This represents the average scattering distribution of all the scattering centers. There does not appear to be a great deal of variation in the general shape of $F(\theta)$, although the average width does change.

3. Scattering coefficient. If we normalize $F(\theta)$, then

$$s = 2\pi \int_0^{\pi} F(\theta) \sin\theta \, d\theta \quad , \tag{1}$$

and

$$f(\theta) = \frac{F(\theta)}{s} \tag{2}$$

is the normalized version. S is the scattering coefficient with s^{-1} interpreted as the average distance between scatterings. Arnush assumed a form for $f(\theta)$ as

$$f(\theta) = \frac{\delta}{2\pi\theta} e^{-\delta\theta} \; ; \delta \cong 10. \tag{3}$$

---

6. Jerlov, N. G., "Optical Oceanography," Elsevier, 1968

7. Duntley, S. Q., "Underwater Lighting by Submerged Lasers," Visibility Laboratory, SIO ref 71-1, June 1971

Heggestad, on the other hand, defines a modified variance

$$\theta^2 = \pi \int_0^{\pi/2} \theta^2 \sin\theta f(\theta) d\theta \approx \frac{1}{\delta^2} \quad , \tag{4}$$

and by equating θ^2 with $1/\delta^2$, the two models are identical. This is true for large δ. We will use the notation θ^2. It is also common to define an extinction coefficient α, defined by

$$\alpha = a + s. \tag{5}$$

Thus, to completely characterize the environment, it would be necessary to have measuring equipment for a, s and $f(\theta)$. An alternate procedure, and a less desirable one, would be to measure two parameters and scale the measurements to the third. Although feasible, this would assume the validity of a model and the confidence to extrapolate from it. With these parameters in mind, we will now present the model.

For convenience we assume that the transmitted beam is Gaussian and has the form

$$f_0(\theta, \underline{r}) = \frac{1}{(\pi\theta_0 r_0)^2} \exp\left[-\frac{\theta^2}{\theta_0^2} - \frac{r^2}{r_0^2}\right] \quad : \tag{6}$$

that is, it has a Gaussian distribution in both its spatial cross section and its ray direction. Next, we assume the geometry in figure 1, where the source is at (0, 0), the observer is at $(\underline{r}, z)$, and as we will see, the apparent source is at $(0, z_0)$. In terms of the observation point $(\underline{r}, z)$ we have as the transfer in intensity $f(\underline{\theta}, \underline{r})$

$$f(\underline{\theta}, \underline{r}) = \frac{1}{(\pi U_r R_0)^2} \exp\left[-az - \frac{(r-r_m)^2}{\chi_0^2} - \frac{\theta_r^2}{U_r^2} - \frac{\theta_\phi^2}{U_\phi^2}\right]$$

$$= \frac{1}{(\pi U_\phi R_1)^2} \exp\left[-az - \frac{(\theta_r - \theta_m)^2 + \theta_\phi^2}{U_\phi^2} - \frac{r^2}{R_1^2}\right] \tag{7}$$

where

$$\begin{aligned}
R_0^2 &= sz^3\theta^2 \left[\frac{1 + 2V + 6\ell + 3\ell V}{3(2 + V)}\right] \\
U_r^2 &= sz\theta^2 (2 + V) \\
U_\phi^2 &= sz\theta^2 \left[\frac{1 + 2V + 6\ell + 3\ell V}{2 + 3(\ell+V)}\right] \\
R_1^2 &= sz^3\theta^2 \left[\frac{2 + 3(\ell + V)}{3}\right]
\end{aligned} \tag{8}$$

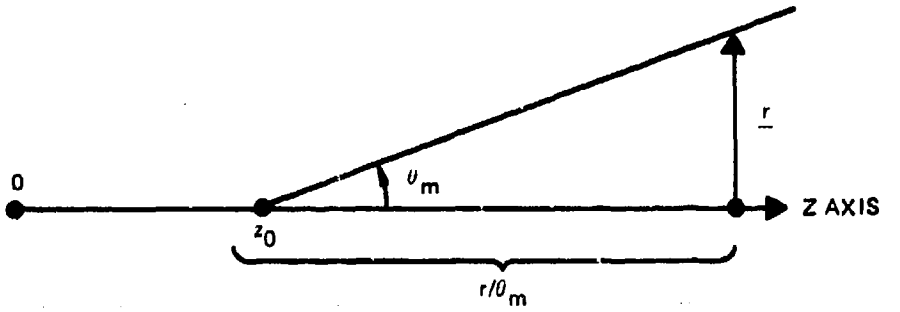

Figure 1. Model geometry.

with

$$\theta_m = \left[\frac{3(1+V)}{2+3(\ell+V)}\right]\left(\frac{r}{z}\right)$$

$$r_m = \left[\frac{1+V}{2+V}\right] \quad z\ U_r \tag{9}$$

and

$$\ell = \frac{r_o^2}{sz^3\overline{\theta^2}} \quad ; \quad V = \frac{\theta_0^2}{sz\overline{\theta^2}} \quad . \tag{10}$$

Some explanation of the interpretation of equation (7) is now warranted. First notice that if we had a receiver at the point ($\underline{r}$, z) and added equally the contributions coming from all angles, we could integrate over the variables θ_r, θ_ϕ and obtain the result*

$$f(\underline{r}) = \int f(\underline{\theta}, \underline{r})\, d\Omega = \frac{e^{-az}}{(\pi R_1^2)} \exp\left[\frac{-r^2}{R_1^2}\right]. \tag{11}$$

Thus, the total energy has a distribution which is Gaussian in the z-plane, is centered at r=0, and is a result of scattering. The standard deviation of this spread is $((R_1^2)/2)^{1/2} = \{(sz^3\overline{\theta^2})/6\,[2+3(\ell+V)]\}^{1/2}$. If in addition we could collect all the scattered radiation in the z-plane (a large collector), we would integrate over r and obtain

*Note: If the ray is coming from the directions $\underline{\theta} = (\theta_r, \theta_\phi)$, then the receiver is pointed in the $(-\underline{\theta}) = (-\theta_r, -\theta_\phi)$ direction. Hence, there is only a sign difference between the two.

$$f = \int f(\underline{r})d\underline{r} = e^{-az} \quad , \tag{12}$$

and identify this as an irretrievable loss which we see is due to absorption.

Now suppose we observe the source at the point ($\underline{r}$, z) as a function of angle (fig 2). Notice $\underline{\mu}_\phi$ is the unit vector in the direction θ_ϕ, the angle out of the r-z plane, and $\underline{\mu}_r$ is the unit vector representing the angular tilt up from the z-axis θ_r in a plane described by $\underline{r}$, z. Thus, for any r, the maximum always occurs in the r-z plane ($\theta_\phi = 0$) at a tilt angle of $\overline{\theta}_m$. Alternatively, for a fixed tilt angle θ_r the maximum occurs when the receiver is off the axis a distance r_m. The net result of both interpretations is that the source appears to be located at the point z_0 (fig 1), where

$$z_o = \frac{z}{3}\left(\frac{1 - 3\ell}{1 + V}\right) . \tag{13}$$

Furthermore, the source will have an apparent extent (size) in diameter (twice the standard deviation) of

$$z^{3/2}(s\overline{\theta}^2)^{1/2}\left\{\frac{2 + 3(\ell + V)}{3(1 + V)}\left(1 + \frac{V}{2}\right)\right\}^{1/2} \tag{14}$$

or

$$2(s\overline{\theta}^2 z)^{1/2} \tag{15}$$

in radians (field of view). Consequently, any system should account for the spatial filtering that may occur when optical elements are used.

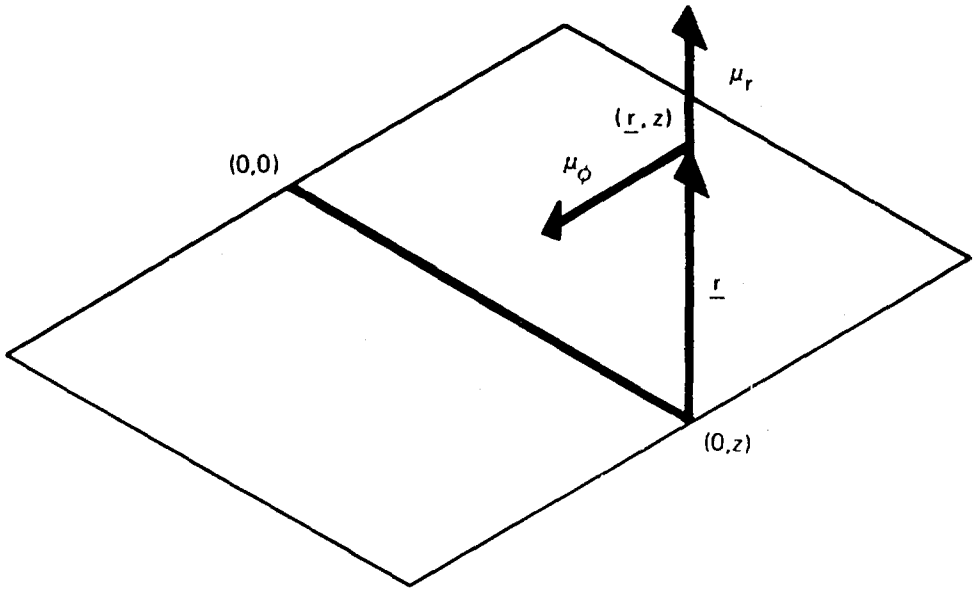

Figure 2. Source as a function of angle.

Finally, we can identify

$$\ell = \frac{r_0^2}{sz^3\theta^2} \sim \frac{r_0^2}{R_1^2} \tag{16}$$

as the ratio of the initial beam cross section to the cross section at ($\underline{r}$, z), which should be much less than one; and

$$V = \frac{\theta_0^2}{sz\theta^2} \sim \frac{\theta_0^2}{U_r^2} \tag{17}$$

as the ratio of the initial beam spread to the beam spread at ($\underline{r}$, z), which should also be much less than one. Thus, we can set $\ell = V = 0$ when collimated beams are used.

Strictly speaking, the model used here is only valid for small-angle forward scatter. This is true because, in the derivation, the approximations $\sin\theta \sim \theta$ and $\cos\theta \sim 1$ are used. However, these approximations are only off by 10–20% at 30–40°, and hence the model should degrade gracefully at larger angles. Some modification has to be made, however, to use this at large angles. This is due to the fact that the absorption and scattering paths are longer by the factor $z[\sec\theta - 1]$ at the angle θ. This can easily be accounted for by changing z to $z\sec\theta = \sqrt{z^2 + r^2}$ wherever z occurs. Then we will interpret equation (7) to be the transfer in intensity from the source to a sphere of radius z. With the latter interpretation in mind we will now show the justification of using this model and then point out the remaining verification needed.

Consider the geometry in figure 3. A collimated source emits radiation along the z-axis. The medium is characterized by the ratio α/a. Since $\alpha = s + a$, $s/a = (\alpha/a) - 1$. The unit of length is $N = \alpha z$ extinction lengths. Thus, N extinction lengths correspond by the relationship.

$$N = \alpha z = \frac{\alpha}{a} az = \left(\frac{\alpha}{a}\right) N_{absorption} \tag{18}$$

to $N/(\alpha/a)$ absorption lengths and, since

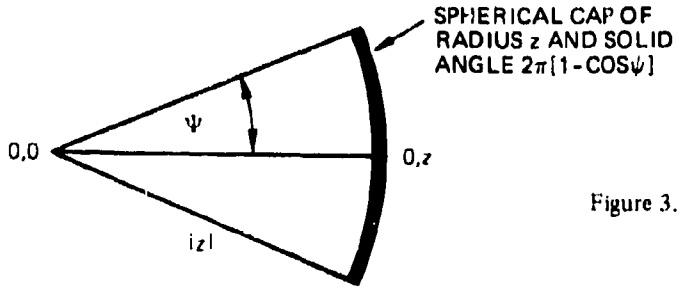

Figure 3. Geometry used by Duntly [7].

$$N_{scat} = sz = [(s+a) - a]z = \alpha z - az = N\left[\frac{\alpha}{a} - 1\right] \qquad (19)$$

to $N[(\alpha/a) - 1]/(\alpha/a)$ scattering lengths.

With this geometry and parameterization, Duntley [ ] has made extensive measurements of the power collected as a function of N for various values of ψ. Two representative samples are shown in figure 4. For this case, equation (11) integrates to

$$\int_0^{\psi z} f(\underline{r})d\underline{r} = e^{-az}\left[1 - e^{\frac{-(\psi z)^2}{R_1^2}}\right]$$

$$= e^{-az}\left[1 - e^{(2/3)s\theta^2 z}\right]$$

$$= e^{-\frac{N}{\alpha/a}}\left[1 - \exp\left\{\frac{-\psi^2}{(2/3)\theta^2 N\left[\frac{\alpha/a-1}{\alpha/a}\right]}\right\}\right]. \qquad (20)$$

As pointed out by Duntley and as observed in equation (12), for large values of ψ we would expect the relationship $e^{-N_{absorption}}$ to hold. However, this is not happening even though the curve saturates for $\psi > 60°$. We can compensate with our model by recalling that the effective source broadens and shifts location as N increases. Duntley was able to observe and measure the former phenomenon, although he was not able to explain it (fig 5). In the actual measurements an integrating sphere was used in the collecting optics. This has a spatial response of $\cos\theta$. Consequently, at large values of N one would expect to start to observe spatial filtering of the source. This is precisely what we see for N greater than 8. This was corrected for as follows. It was assumed that the difference between the $e^{-N_{absorption}}$ line and the $\psi = 100°$ curve was due to spatial filtering. Therefore, at every value of N this difference was added to each of the curves (on a log scale) and replotted. The model was then calibrated at the largest value of N and the smallest value of ψ, where it should be most accurate, and θ^2 was calculated. The model was then plotted on the revised curves (fig 6). Although the agreement is not perfect, it is remarkably close. The validity of this calibration should be checked at some point by comparing the results of an integrating sphere with those of a hemispherical coverage lens (fisheye).

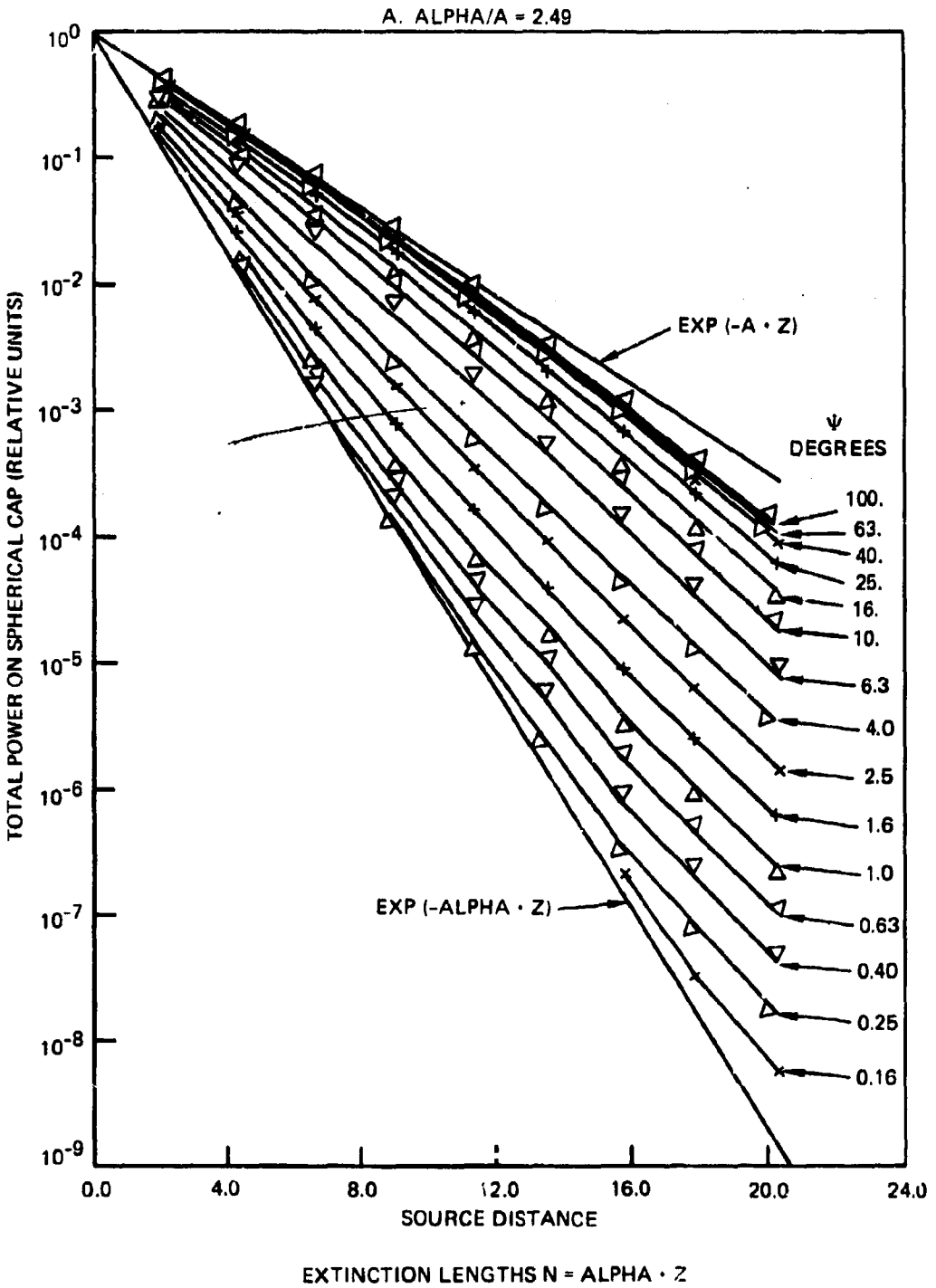

Figure 4. Total power on spherical cap.

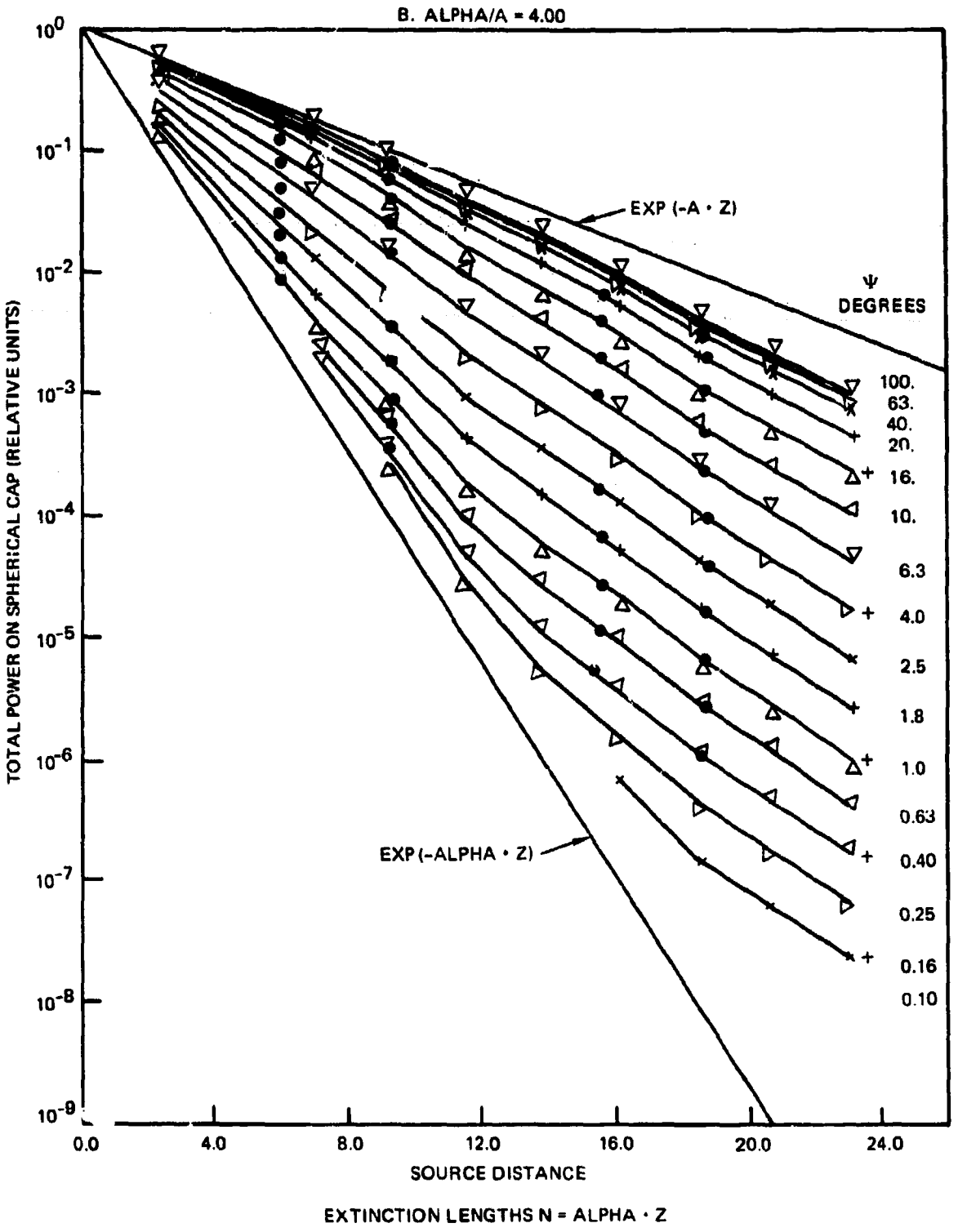

Figure 4. (Continued).

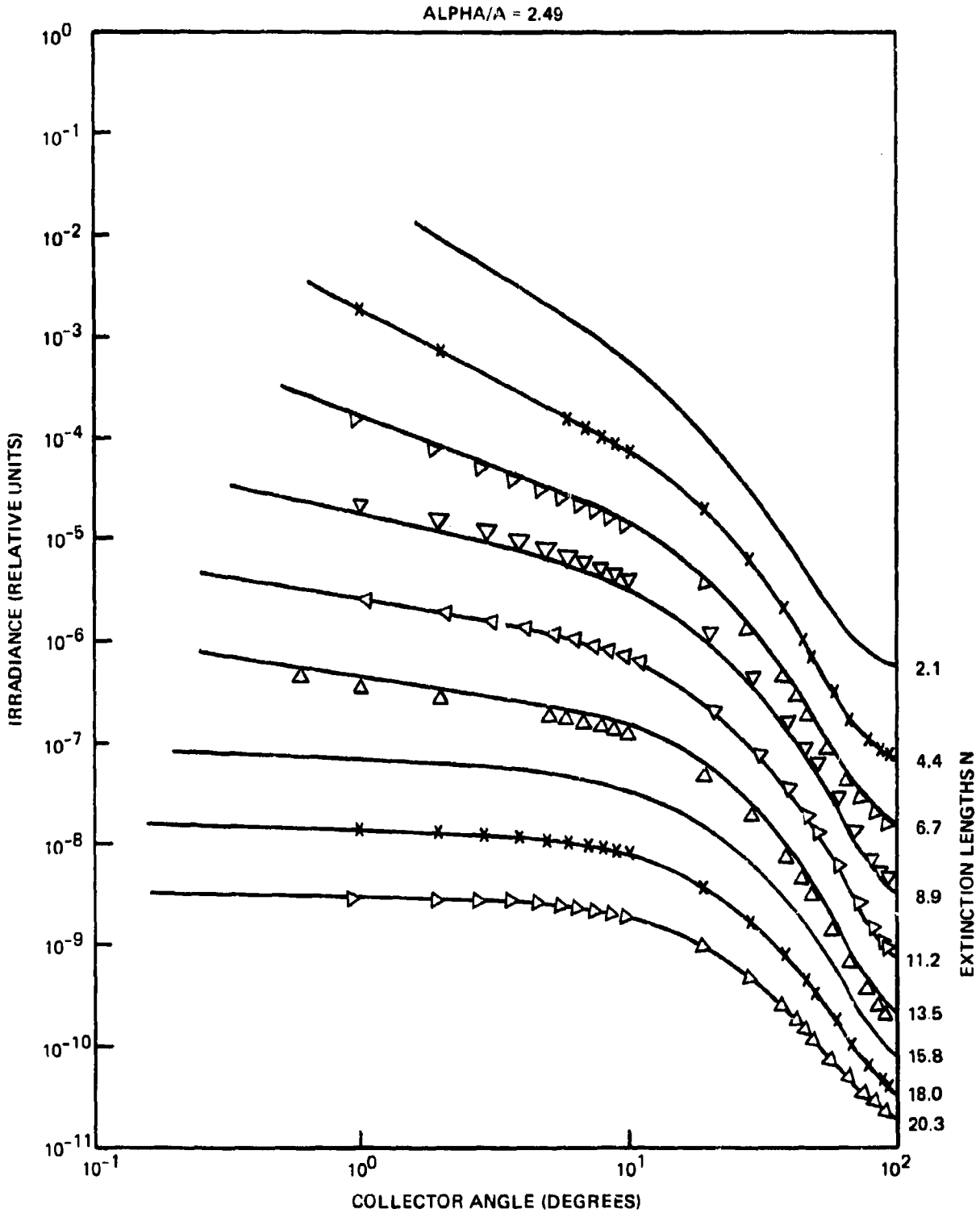

Figure 5. Duntley measurements of anomalous model behavior.

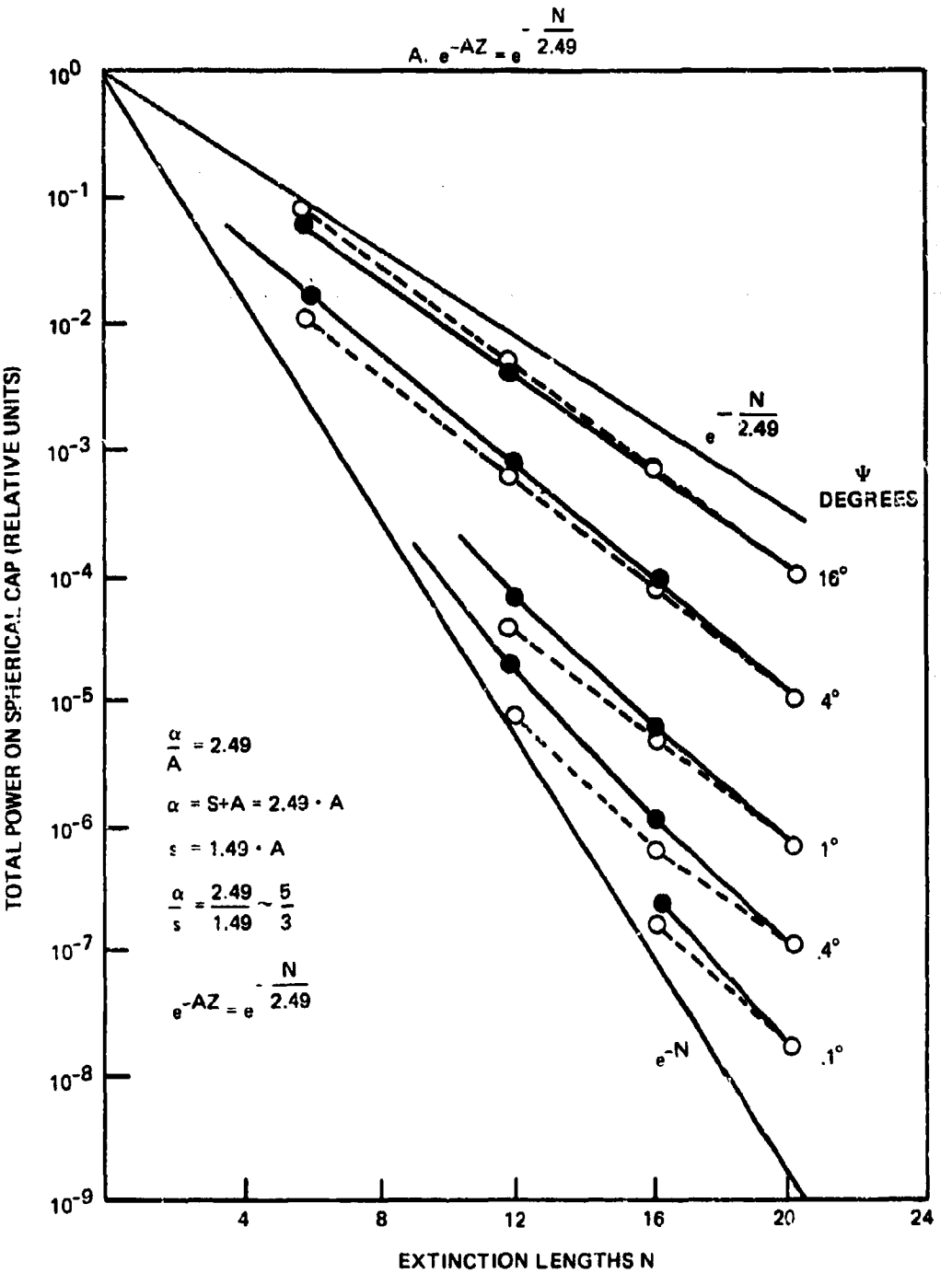

Figure 6. Revised model curves.

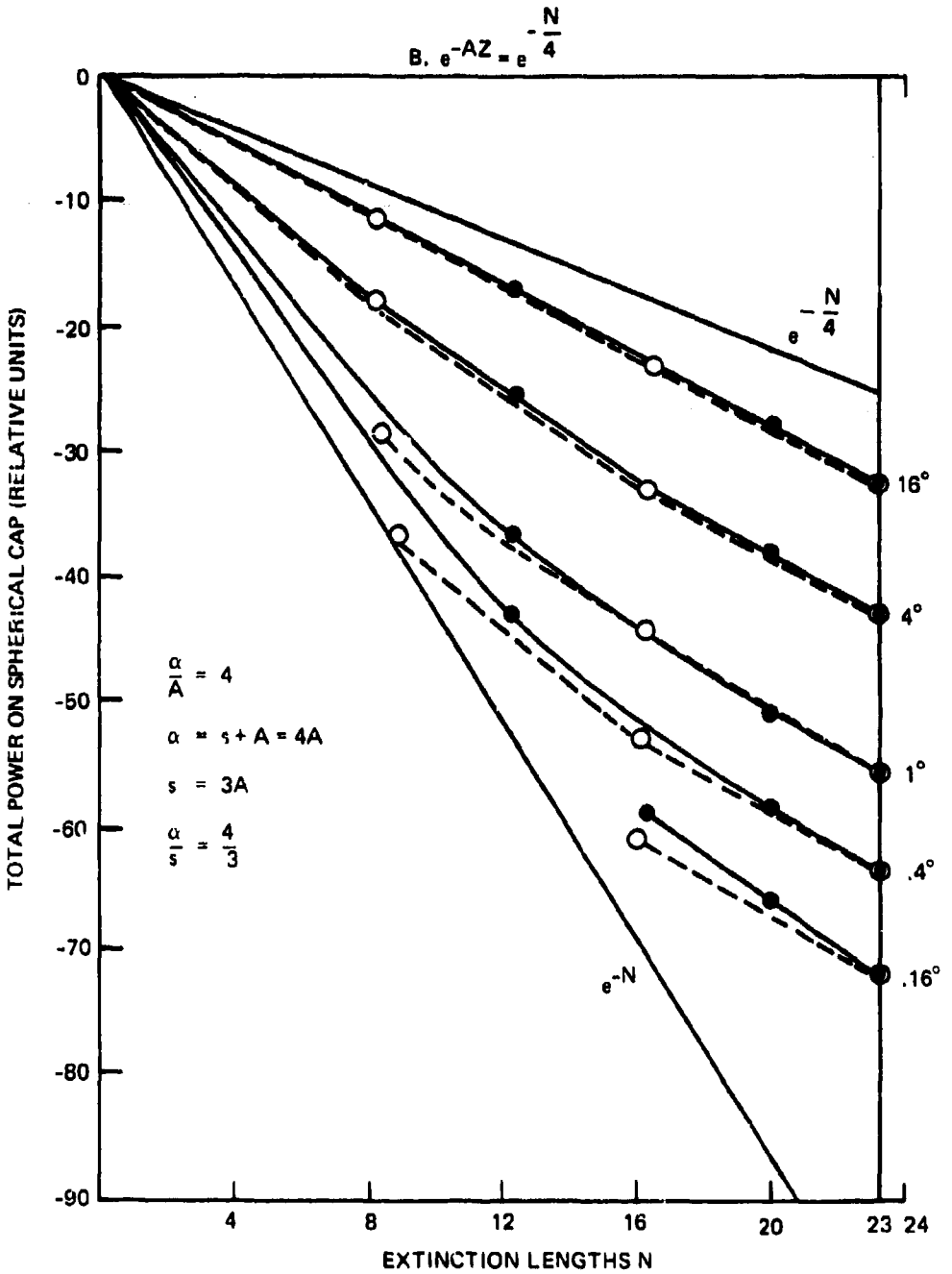

Figure 6. (Continued).

THE AIR/SEA INTERFACE

In this section a geometric optics model is developed to determine the effect of surface irregularities on beam spreading, pointing, and scintillation in traversing the boundary. To do so, we consider the following model of an element of the surface (fig 7). A ray of light, γ degrees off the normal, impinges upon the surface whose local slope is R degrees from the horizontal. By Snell's law

$$n' \sin(\gamma' + R) = n \sin(\gamma + R) \tag{21}$$

and

$$\gamma' = \sin^{-1}\left[\frac{n}{n'} \sin(\gamma + R)\right] - R\,, \tag{22}$$

which is valid for both positive and negative slopes. γ and γ' are always taken with respect to the true vertical. If R is a random variable, the statistics of the slope must also be factored in. We do this in the following manner. Given a sample R from the set of possible slopes, γ' is well defined. That is, the probability of γ' conditioned upon γ and R is

$$p(\gamma'/\gamma, R) = \delta[\gamma' - (\sin^{-1}\left(\frac{n}{n'} \sin(\gamma+R)\right) - R)]\,. \tag{23}$$

We arrive at the angular distribution of γ', given γ, by averaging over the variable R. Thus,

$$p(\gamma'/\gamma) = \int_{-\infty}^{\infty} dR\, p_R(R)\, p(\gamma'/\gamma, R)$$

$$= \int_{-\infty}^{\infty} dR\, p_R(R)\delta\,[\gamma' - (\sin^{-1}\left(\frac{n}{n'} \sin(\gamma+R)\right) - R)]\,, \tag{24}$$

where $p_R(R)$ is the probability density of R.

Rigorously, this is merely the change of variables in the density $p_R(R)$ from R to γ' by use of

$$R = \tan^{-1}\left[\frac{\frac{n}{n'} \sin\gamma - \sin\gamma'}{\cos\gamma' - \frac{n}{n'}\cos\gamma}\right] = R(\gamma', \gamma)\,. \tag{25}$$

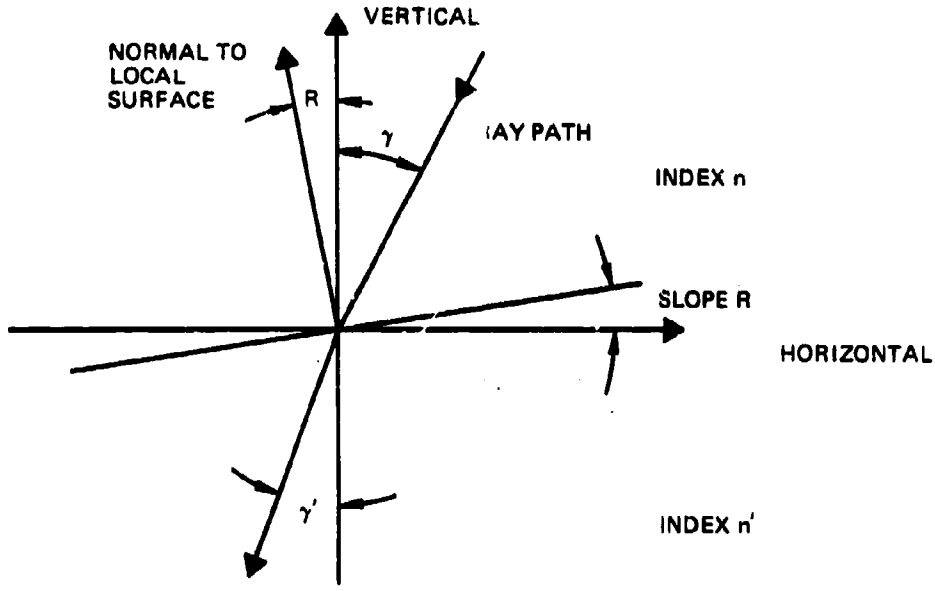

Figure 7. Model of an element of the surface.

Thus,

$$p(\gamma'/\gamma) = p_R\,[R(\gamma', \gamma)] \left| \frac{dR(\gamma', \gamma)}{d\gamma'} \right|$$

$$= p_R \left[\frac{\frac{n}{n'} \sin\gamma - \sin\gamma'}{\cos\gamma' - \frac{n}{n'} \cos\gamma} \right] \left| \frac{\frac{n}{n'} \cos(\gamma - \gamma') - 1}{\cos^2\gamma' + \left(\frac{n}{n'}\right)^2 \cos^2\gamma - 2\frac{n}{n'} \cos\gamma \cos\gamma'} \right| \quad (26)$$

Knowing $p(\gamma'/\gamma)$, we can compute the average spreading and offset of a ray incident at the angle γ. This becomes

$$\text{average offset} = \int \gamma'\ p(\gamma'/\gamma)\, d\gamma' = \overline{\gamma'}$$

$$= \int \left\{ \sin^{-1}\left[\frac{n}{n'} \sin(\gamma + R)\right] - R \right\}\ p_R(R) dR$$

$$= \int \sin^{-1}\left[\frac{n}{n'} \sin(\gamma + R)\right]\ p_R(R) dR - \overline{R} \quad . \quad (27)$$

With $\overline{\gamma'^2}$ defined as

$$\overline{\gamma'^2} = \int \gamma'^2\, p(\gamma'/\gamma)d\gamma'$$

$$= \int \left\{ \sin^{-1}\left[\frac{n}{n'}\sin(\gamma + R)\right] - R \right\}^2 p_R(R)dR, \tag{28}$$

the rms spread becomes

$$\Delta = (\overline{\gamma'^2} - \overline{\gamma'}^2)^{1/2} \tag{29}$$

There are some practical limitations to these results which require modification (fig 8). A ray of light with zenith angle γ will never intercept a wave whose slope is greater than $(\pi/2) - \gamma$ because of wave obscuration. However, the ray will still penetrate the interface with probability one. Consequently, the limits of integration for R are set at $[-(\pi/2), (\pi/2) - \gamma]$ and the density $p_R(R)$ should be modified to that of

$$\frac{p_R(R)}{\int_{-\pi/2}^{\pi/2-\gamma} p_R(R)dR} = \begin{cases} \hat{p}_R(R) \; ; \; -\pi/2 \leq R \leq \pi/2 - \gamma \\ 0 \text{ elsewhere} . \end{cases} \tag{30}$$

The results in equations (26-29) would then be modified by replacing $p_R(R)$ with $\hat{p}_R(R)$. In general, the results presented can be simplified by only considering those values of $(\gamma + R) < 45°$. This corresponds to the major operational requirements and gives good engineering insight into the behavior of a ray going through the air/sea interface. For this case

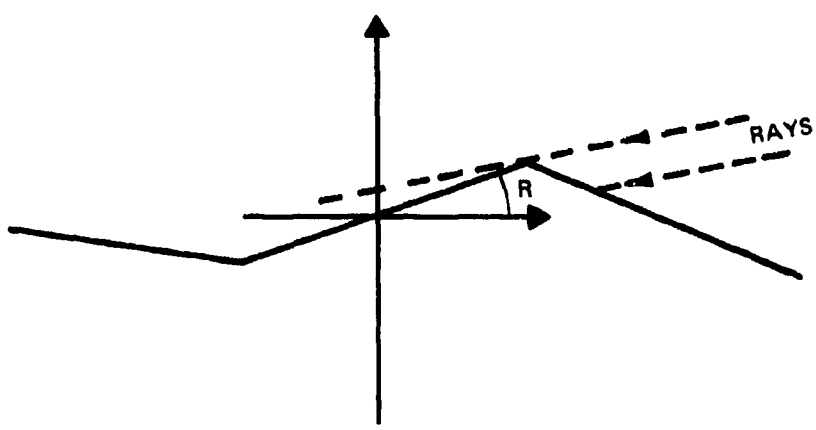

Figure 8. Modifications of model.

$$p(\gamma'/\gamma) \approx p_R\left[\frac{\frac{n}{n'}\gamma - \gamma'}{1 - \frac{n}{n'}}\right] \left|\frac{1}{1 - \frac{n}{n'}}\right|$$

$$\overline{\gamma'} \approx \frac{n}{n'}\gamma + \left(1 - \frac{n}{n'}\right)\overline{R} \tag{31}$$

$$\Delta^2 \approx \left|1 - \frac{n}{n'}\right|^2 \text{ var } [R] \ .$$

Notice that $|1 - n/n'|^2 < 1$ for the air/sea interface (index of water = 1.33, index of air = 1), and consequently the ray spreading is appreciably less than the slope spreading of the ocean. In addition, the surface adds the contribution of $(1 - n/n')\overline{R}$ to the normal bending due to Snell's law.

In all cases, the model used represents an optical beam of zero cross section and zero divergence. The exiting beam also has zero cross section and zero divergence but is being steered by the roughness of the surface. If this surface is the ocean, $p(\gamma'/\gamma)$ represents the average time history of the beam direction γ', with $p(\gamma'/\gamma)d\gamma'$ the probability that it is pointing within a $d\gamma'$ interval of the γ' direction at any instant in time. This apparent beam wander would cause severe scintillation in an operating system. As the cross section of the beam increases, the refracting surface can no longer be considered locally flat, and different portions of the beam are refracted at different angles. Consequently, it would be possible to average out the beam wander in the direction of the mean $\overline{\gamma}'$ by spreading the beam over a larger portion of the surface. If the area of the beam is A and the correlation length of the surface statistics is L, then there are approximately $A/(\pi L/2)^2$ identically distributed independent paths similar to diversity paths. If we further assume a depth z such that the beam cross section is greater than A,

$$\frac{sz^3\theta^2}{3} > A, \tag{32}$$

then all the paths will overlap at the receiver. This can be analysed in the following manner. First we notice that the probability of having the beam within an rms deviation about the mean is

$$\int_{\overline{\gamma}' - \Delta}^{\overline{\gamma}' + \Delta} p(\gamma'/\gamma)d\gamma' \tag{33}$$

which for the Gaussian density becomes 0.68. Thus, even if we had no time variations, the beam would be within a deviation of the mean only 68% of the time. Now suppose we pick N independent, identically distributed paths to the receiver and transmit $(1/N)^{th}$ of the power p_i in each path. Since the paths are identically distributed, the average direction of the sum is still $\overline{\gamma}'$. Now, however, the variance of the sum becomes Δ^2/N, or a standard deviation for the sum of $\Delta/\sqrt{N}$ about the mean $\overline{\gamma}'$. If, for example, we set N = 25, and assume

the central limit is approximately valid, the probability that the beam is within $\pm\Delta$ is now 0.999994. Since the correlation length is approximately the separation between independent spatial Nyquist samples, we see that

$$N \sim \frac{A}{\pi\left(\frac{L}{2}\right)^2} \tag{34}$$

and can be used accordingly. Furthermore, it can be shown that the scintillation will reduce the average signal-to-noise ratio by the factor

$$\frac{1}{1 + \Delta^2/N} \quad . \tag{35}$$

A verification of these results and the relationship in equation (32) would be warranted.

Finally, we can interpret the function $p(\gamma'/\gamma)$ as a beam-spreading factor. Thus, if we have a propagating beam of the form $f(\theta, r)$ in equation (7), or $f(\gamma, r)$, then the output beam after traversing the surface will be

$$f(\gamma', r) = \int d\gamma p(\gamma'/\gamma) f(\gamma, r), \tag{36}$$

or an average over all input ray directions weighted by the relative intensity. Notice that we have not restricted the results to which medium corresponds to air and which to water. When going from air to water, set $n = 1$, $n' = 1.33$; and when going from water to air, set $n = 1.33$ and $n' = 1$. Then the computation of the beam moments after traversing the surface yields

$$\overline{\gamma'} = \frac{\int \gamma' f(\gamma', r)\, d\gamma'}{\int f(\gamma', r) d\gamma'}$$

$$\text{var}\,|\gamma'| = \frac{\int (\gamma' - \overline{\gamma'})^2 f(\gamma', r) d\gamma'}{\int f(\gamma', r) d\gamma'} \quad . \tag{37}$$

The results derived in this section were performed for a one-dimensional surface. To extend them to a two-dimensional surface is straightforward if we restrict ourselves to Cartesian coordinates. The variable R would then become the pair $\underline{R} = (x, y)$, and the one-dimensional results would carry over to each of the orthogonal coordinates. The interpretation would then be one of projecting the true slope distribution onto the Cartesian coordinate system. Although simple in theory, the actual computations are difficult. If we use the linearization implicit in equation (31), this problem is greatly simplified. For this reason we will restrict our analysis to this assumption. To make the calculations for large zenith angles, a more rigorous assessment of the surface geometry must be performed [8].

8. Swennen, J. P. J. W., "Time-Average Power-Density Probability Distribution below the Ocean Surface of a Beam of Collimated Optical Radiation Incident on the Surface," JOSE 56, p 224-229, 1966

SATELLITE TO SUBMERGED PLATFORM

The computation of satellite to submerged platform power budget is aided by a brief discussion of the geometry. It is assumed, for a variety of reasons, that we will project a spot on the ocean approximately 1 mile in diameter. Thus, if we transmit p_t watts of radiation, from the zenith the full angle of the beam will be approximately (1/22000) radians $\approx$ 50 μrad = 10 s. The power density (intensity) at the surface will be approximately

$$\frac{P_t}{\pi(830)^2} = 4.62 \times 10^{-7} P_t \text{ W/m}^2. \tag{38}$$

If the surface is illuminated at an angle γ from the zenith, then the power density will be

$$\frac{P_t \cos\gamma}{\pi(830)^2} = 4.62 \times 10^{-7} P_t \cos\gamma \text{ W/m}^2. \tag{39}$$

Now, however, the circular spot has elongated into an ellipse with minor axis 830 m and major axis (830/cos γ)m. We will use the symmetry along the major axis of the ellipse to pick a convenient coordinate system. We will call this the x-axis. The minor axis will define the y-axis of the coordinate system and the depth of the ocean will constitute the z-axis (fig 9).

In practice, the spot will have a nonuniform illumination. We will account for this by defining a normalized intensity $I(x_0, y_0)$, which we then multiply by the factor in equation (38).* Notice that the angle γ is always measured between the x-y plane and a line in the x-z plane. This will allow us to use the second form in equation (7). At any location (x_0, y_0) in the x-y plane an elementary surface element x_0, y_0 contributes an amount $I(x_0, y_0)dx_0dy_0$. A ray with this intensity passing through the air/sea interface yields the value

$$f(\underline{\gamma}'; (x - x_0), (y - y_0)) = I(x_0, y_0)\, dx_0dy_0\, p(\underline{\gamma}'/\underline{\gamma}) \tag{40}$$

as the intensity on the water side of the boundary. At this point we will consider a functional form for $p(\underline{\gamma}'/\underline{\gamma})$ to aid in the computation. From experimental results [10] it

---

* To be correct, the transmission coefficient at the boundary should also be included as a function of angle [9].

9. Stratton, J. A., "Electromagnetic Theory," McGraw Hill, 1941.

10. Cox, C., and Munk, W., Bulletin Scripps Inst Oceanog Univ California 6 401, 1956.

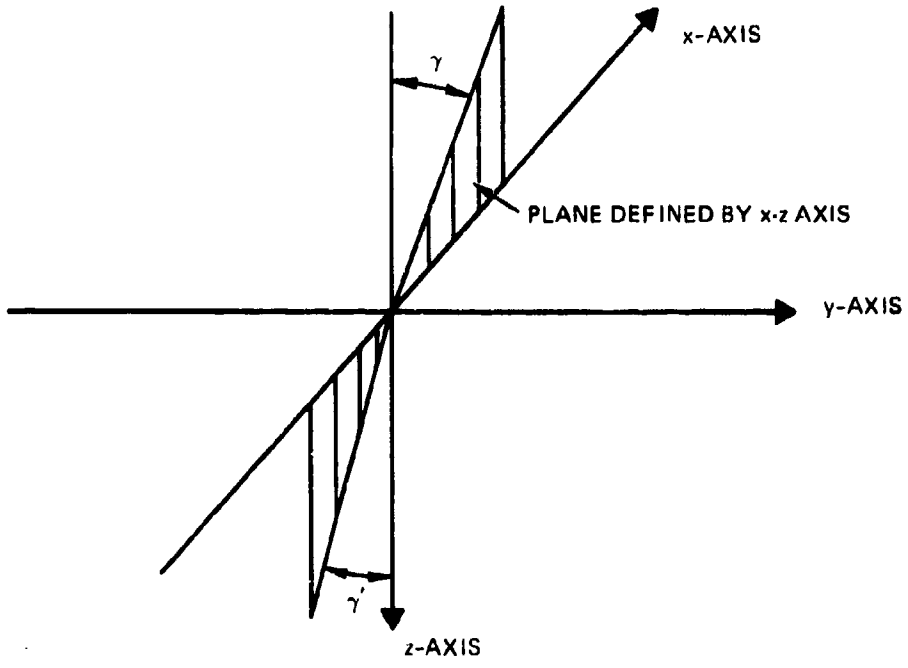

Figure 9. Axes of coordinate system.

can be assumed that $p(\underline{\gamma}'/\underline{\gamma})$ is Gaussian. Furthermore, if we keep to angles such that equation (31) is valid, then*

$$p(\underline{\gamma}'/\underline{\gamma}) = \frac{\exp - \left[\frac{\left|\gamma' - \left\{\frac{n}{n'}\underline{\gamma} + \left(1 - \frac{n}{n'}\right)\overline{R}\right\}\right|^2}{2\left[1 - \frac{n}{n'}\right]^2 \text{var}\,[R]}\right]}{2\pi\left|\left|1 - \frac{n}{n'}\right|^2 (\text{var}\,[R])\right|}. \tag{41}$$

For this approximation

$$f(\underline{\gamma}'; (x-x_0), (y-y_0)) = \frac{I(x_0, y_0)\, dx_0 dy_0}{2\pi\left|\left|1 - \frac{n}{n'}\right|^2 (\text{var}\,[R])\right|} \exp - \left[\frac{\left|\underline{\gamma}' - \left\{\frac{n}{n'}\underline{\gamma} + \left(1 - \frac{n}{n'}\right)\overline{R}\right\}\right|^2}{2\left[1 - \frac{n}{n'}\right]^2 \text{var}\,[R]}\right]. \tag{42}$$

* To use correlated Gaussian variables would only be the refinement of an approximation.

Inserting this into equation (7) and using the off-axis correction to the intensity, we find at a point below the surface that the contribution from the intensity $I(x_0, y_0)$ in an area dx_0dy_0 at the point $(x_0, y_0, 0)$ to the intensity at (x, y, z) is

$$\Delta I(x, y, z; \gamma'_x\gamma'_y) = \frac{I(x_0, y_0)\, dx_0dy_0}{(\pi U'^2_\phi R'^2_1)} \exp - \left\{ a[z^2 + (x_0 - x)^2 + (y_0 - y)^2]^{1/2} + \left[\frac{\xi_x^2 + \xi_y^2}{R'^2_1}\right] + \frac{1}{U'^2_\phi}\left[(\gamma'_x - \overline{\gamma}_x)^2 + (\gamma'_y - \overline{\gamma}_y)^2 + \theta'^2_m - 2\theta'_m \left\{ \frac{(x_0 - x)(\gamma'_x - \overline{\gamma}_x)}{\sqrt{(x_0 - x)^2 + (y_0 - y)^2}} - \frac{(y_0 - y)(\gamma'_y - \overline{\gamma}_y)}{\sqrt{(x_0 - x)^2 + (y_0 - y)^2}} \right\}\right]\right\}, \quad (43)$$

where

$$\theta'_m = \frac{3(1 + V')}{2 + 3(\ell' + V')}\left[\frac{\sqrt{\xi_x^2 + \xi_y^2}}{\sqrt{z^2 + (x_0 - x)^2 + (y_0 - y)^2}}\right]$$

$$R'^2_1 = s[z^2 + (x_0 - x)^2 + (y_0 - y)^2]^{3/2}\,\overline{\theta^2}\left[\frac{2 + 3(\ell' + V')}{3}\right]$$

$$U'^2_\phi = s[z^2 + (x_0 - x)^2 + (y_0 - y)^2]^{1/2}\,\overline{\theta^2}\left[\frac{1 + 2V' + 6\ell' + 3\ell'V'}{2 + 3(\ell' + V')}\right] \quad (44)$$

with

$$V' = \frac{\left(1 - \frac{n}{n'}\right)^2 \mathrm{var}[R]}{s\overline{\theta^2}[z^2 + (x_0 - x)^2 + (y_0 - y)^2]^{1/2}}$$

$$\ell' = \frac{\Delta x_0 \Delta y_0}{s\overline{\theta^2}[z^2 + (x_0 - x)^2 + y_0 - y)^2]^{3/2}} \approx 0$$

$$\overline{\gamma}_x = \frac{n}{n'}\gamma + \left(1 - \frac{n}{n'}\right)\overline{R}_x$$

$$\overline{\gamma}_y = \left(1 - \frac{n}{n'}\right)\overline{R}_y \quad (45)$$

$$\xi_x^2 = \left\{ -\bar{\gamma}_x + \sin^{-1} \frac{(x_0 - x)}{\sqrt{z^2 + (x_0 - x)^2}} \right\}^2 (z^2 + (x_0 - x)^2)$$

$$\xi_y^2 = \left\{ -\bar{\gamma}_y + \sin^{-1} \frac{(y_0 - y)}{\sqrt{z^2 + (y_0 - y)^2}} \right\}^2 (z^2 + (y_0 - y)^2) \quad . \tag{46}$$

In equation (43) we have introduced the new variables γ'_x and γ'_y. The former is the angle measured in the x-z plane while the latter is the angle perpendicular to the x-z plane. This set of variables results from a rotation of coordinates of the variables θ_r and θ_ϕ by the transformation

$$\theta_\phi = \frac{(y_0 - y)}{\sqrt{(y_0 - y)^2 + (x_0 - x)^2}} \gamma'_x + \frac{(x_0 - x)}{\sqrt{(y_0 - y)^2 + (x_0 - x)^2}} \gamma'_y$$

$$\theta_r = \frac{(x_0 - x)}{\sqrt{(y_0 - y)^2 + (x_0 - x)^2}} \gamma'_x - \frac{(y_0 - y)}{\sqrt{(y_0 - y)^2 + (x_0 - x)^2}} \gamma'_y \quad . \tag{47}$$

The necessity for this rotation arises from the fact that θ_r lies in the plane described by the points (x_0, y_0), (x, y) and the refracted angle. Consequently, it is necessary to project the angular contributions onto a common set of coordinates before integration. Since the transformation is unitary, the variables γ'_x and γ'_y are still normalized to one. Finally, we see that

$$I(x, y, z; \gamma'_x, \gamma'_y) = \int_{-\infty}^{\infty}\int \Delta I\,(x, y, z)\, dx_0 dy_0. \tag{48}$$

It is evident that, even with the simplifying assumptions used, the model is complicated. Therefore, in terms of an experiment, it is important to pick a geometry such that we can make further simplifying assumptions. For example, an experiment using the sun at zenith would have $\underline{\gamma} = 0$, $I(x_0, y_0) =$ constant, $x = y = 0$. We could also pick a calm day so that we can assume $\bar{R}_x = \bar{R}_y = V' = 0$. If in addition we collect over a sphere with a fisheye lens, we have

$$\frac{I(0, 0, z)}{I(x_0, y_0, z)} = \int_{-\infty}^{\infty}\int \frac{1}{\pi R_1'^2} \exp - \left\{ a[z^2 + x_0^2 + y_0^2]^{1/2} - \frac{(\xi_x^2 + \xi_y^2)}{R_1'^2} \Big|_{x=y=\bar{\gamma}_x=\bar{\gamma}_y=0} \right\} dx_0 dy_0$$

$$R_1'^2 = (2/3)s\theta^2[z^2 + x_0^2 + y_0^2]^{3/2} \quad . \tag{49}$$

Setting $x_0 = r_0 \cos\rho$, $y_0 = r_0 \sin\rho$ and assuming

$$\sin^{-1} \frac{x_0}{\sqrt{z^2 + x_0^2}} \approx \frac{x_0}{\sqrt{z^2 + x_0^2}}$$

and

$$\sin^{-1} \frac{y_0}{\sqrt{z^2 + y_0^2}} \approx \frac{y_0}{\sqrt{z^2 + y_0^2}} ,$$

we have

$$\frac{I(0, 0, z)}{I(x_0, y_0)} = 2 \int_0^\infty \frac{\exp - \left\{ a[z^2+r_0^2]^{1/2} + \dfrac{r_0^2}{(2/3)s\overline{\theta^2}[z^2+r_0^2]^{3/2}} \right\}}{(2/3)s\overline{\theta^2}[z^2 + r_0^2]^{3/2}} r_0 dr_0 . \qquad (50)$$

(Notice that for $z = 0$ the approximation $1' = 0$ does not hold.)

The power collected at depth z will be merely $AI(0, 0, z)$, where A is the size of the collecting aperture. Consequently, a measurement of $I(0, 0, z)/I(x_0, y_0)$ over many extinction lengths would indicate the validity of extrapolating the model to great depths.

We have now presented three separate methods for computing the power loss to a depth z when the source is at the zenith and no other effects are considered. By order of expected accuracy, they are equation (49), equation (50) and equation (7), when the beam radius r_0 is considered large. In figure 10 we plot equation (50) as a function of the upper limit of integration. Notice that in all cases convergence occurs when the radius is approximately z/2 for $\overline{\theta^2} = 0.01$. As $\overline{\theta^2}$ increases from 0.01 to 0.11, the effective surface area increases and the total contribution decreases. A calculation of equation (49) was also made and the result was within a few percent of that calculated by equation (50) for $\overline{\theta^2} = 0.01$. Finally, when we use equation (7) with r_0 large, it can easily be shown that $I(0, 0, z)/I(x_0, y_0)$ is merely e^{-az}. This is plotted together with the previous results in figure 11 as a function of z. At 300 m and $\overline{\theta^2} = 0.01$ the difference was only 3 dB. This result implies that the diffuse reflection coefficient [6] when measured at the zenith is approximately the absorption coefficient.

In a practical system, one will encounter background noise arising from the sky and the sun. When this occurs, the use of a 4π steradian collector will admit an unacceptable amount of noise into the detector circuitry. For these cases it can be shown that to optimize the received signal-to-noise ratio, a spatially matched filter should be used. Simply stated, the matched filter will take two forms depending upon whether we have blue sky or the sun (or both). To eliminate a source such as the sun, the filter reduces to an obscuration covering the field of view subtended by the sun to the receiver. For an extended source, the filter takes on the angular distribution subtended by the source to the receiver. In practice this reduces to an obscuration which only passes that portion of the field in which the

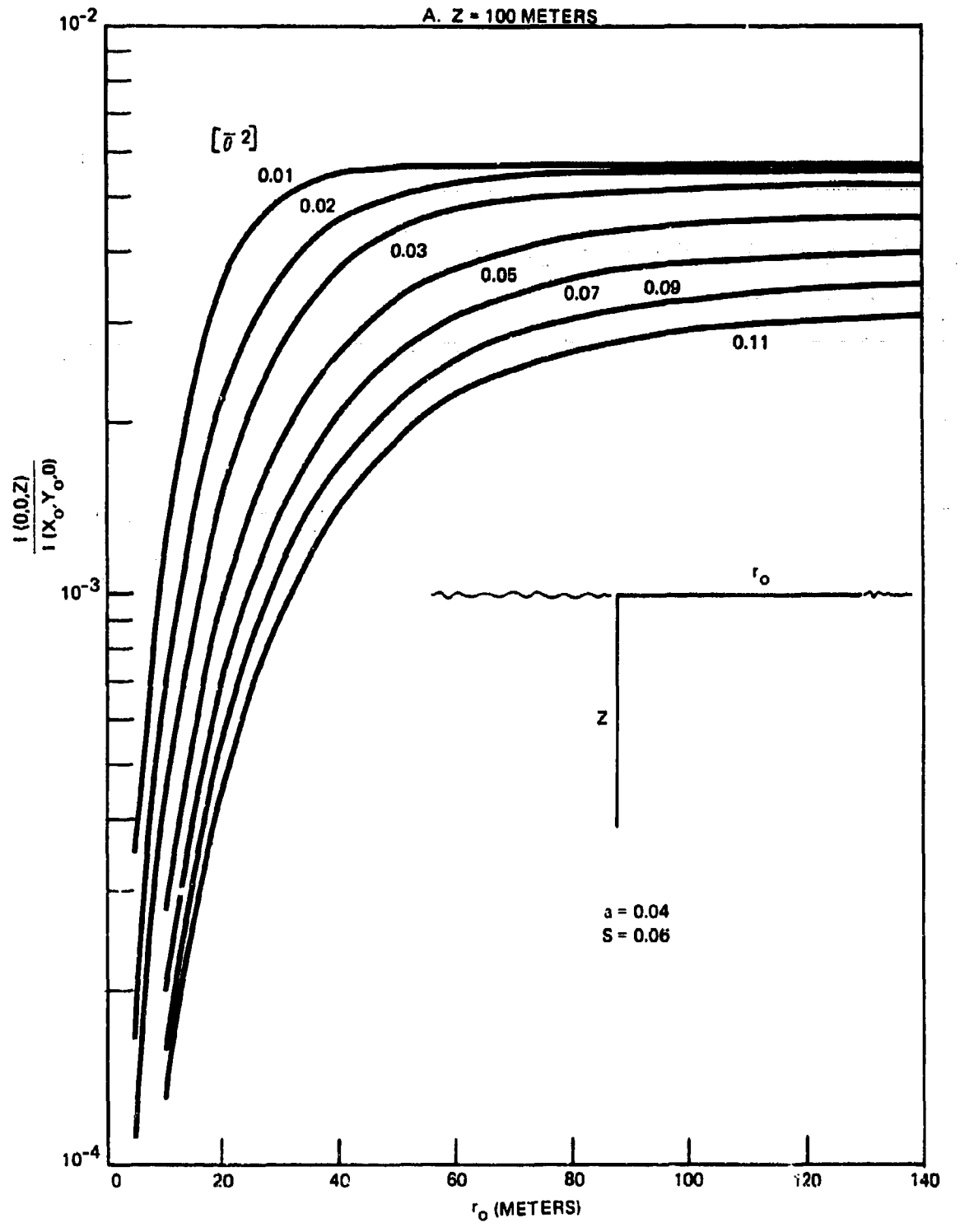

Figure 10. Equation (50) plotted as a function of the upper limit of integration.

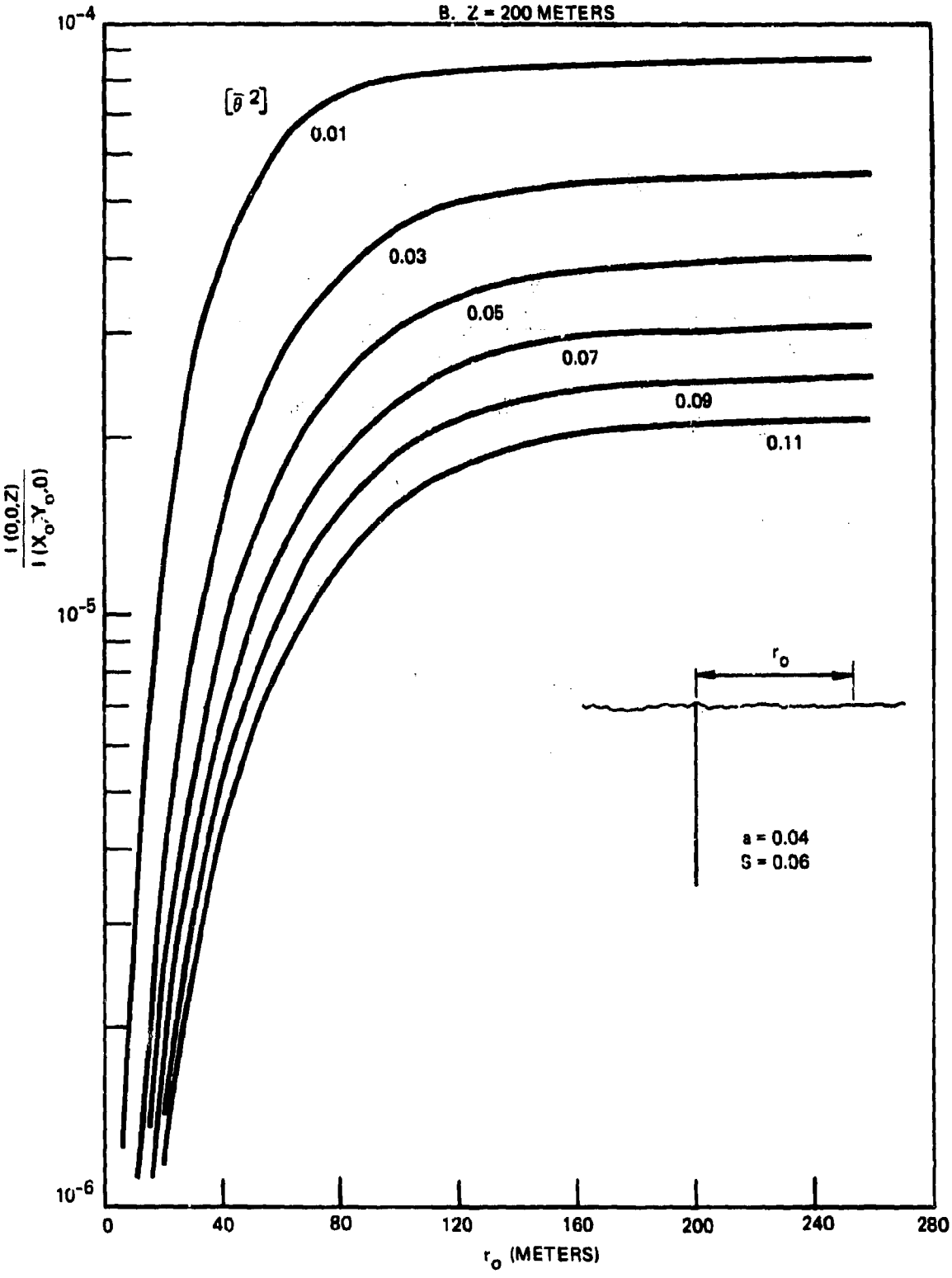

Figure 10. (Continued).

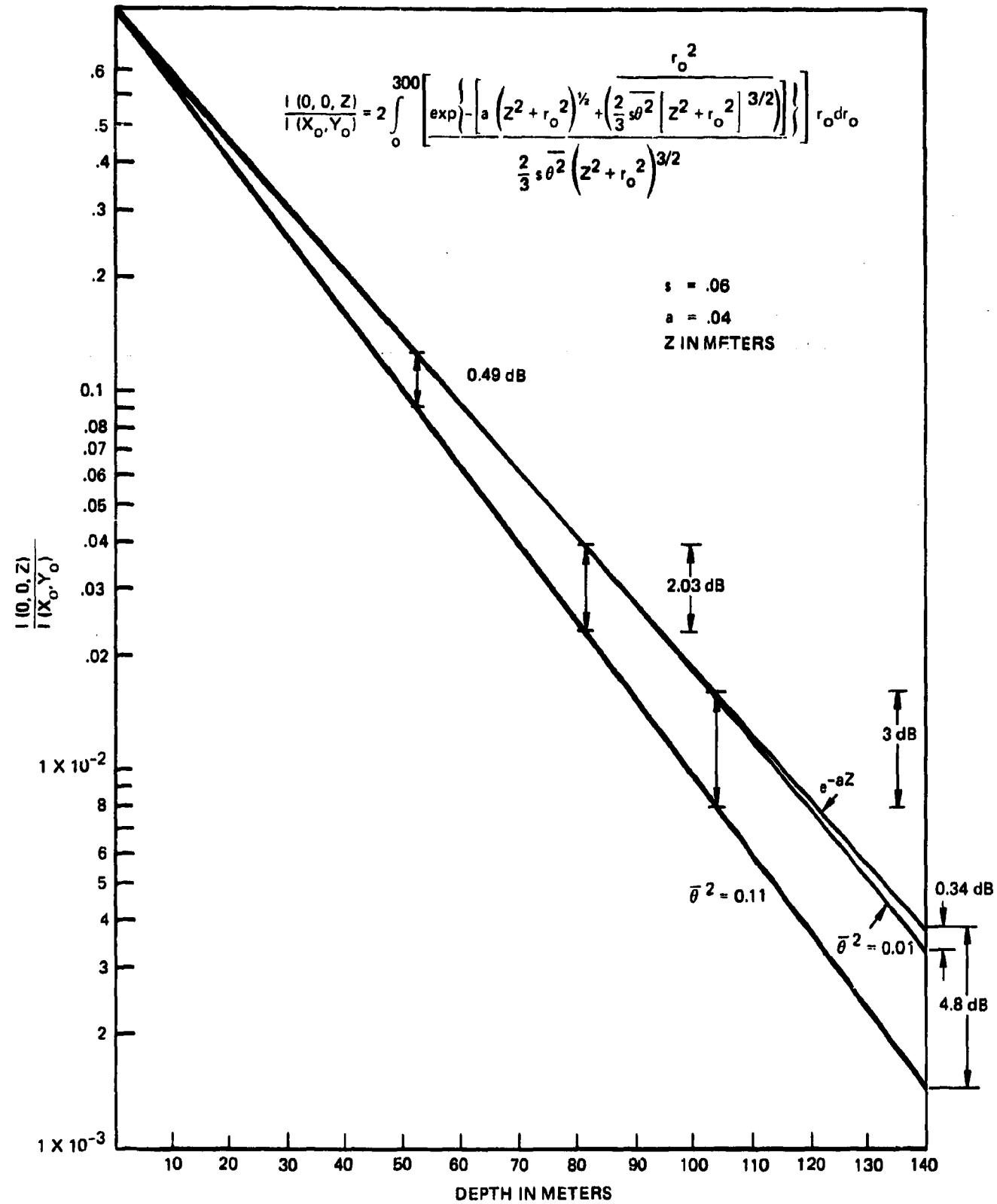

Figure 11. Equation (7) plotted with r_o large.

major portion of the source subtends. Mathematically, we would integrate equation (48) over the variables γ'_x and γ'_y with the integration boundary determined by the receiver field of view. Then equation (43) could be rewritten as

$$\Delta I(x, y, z; \gamma'_x, \gamma'_y) = \frac{I(x_0, y_0)\, dx_0 dy_0}{(\pi U'^2_\phi R'^2_1)} \exp$$

$$- \left\{ a[z^2 + (x - x_0)^2 + y - y_0)^2]^{1/2} \right.$$

$$+ \left[\frac{\xi_x^2 + \xi_y^2}{R'^2_1} \right] + \frac{1}{U'^2_\phi} \left[\left(\gamma'_x - \overline{\gamma}_x \right. \right.$$

$$\left. - \frac{(x_0 - x)\theta'_m}{\sqrt{(x_0 - x)^2 + (y_0 - y)^2}} \right)^2 .$$

$$\left. \left. + \left(\gamma'_y - \overline{\gamma}_y + \frac{(y_0 - y)\, \theta'_m}{\sqrt{(x_0 - x)^2 + (y_0 - y)^2}} \right)^2 \right] \right\}. \qquad (51)$$

And, if we assume that the receiver will be pointing at the refracted angle $(n/n')\gamma$, we can perform the integration over a finite field of view between say $n/n'\gamma - \Delta$ and $n/n'\gamma + \Delta$. If we perform the integration over a cone, we find that some difficulty would arise in trying to obtain a closed-form solution. However, by referring to figure 12, we see that upper and lower bounds can easily be obtained in closed form. The resultant received power over the finite field of view Ω can be obtained by using combinations of the function

$$I(x, y, z, \Omega) = \int_{x_0} \int_{y_0} \frac{I_0(x_0, y_0)\, dx_0 dy_0}{\pi R'^2_1} \left[\exp \right.$$

$$\left. - \left\{ a[z^2 + (x - x_0)^2 + (y - y_0)^2]^{1/2} + \frac{(\xi_x^2 + \xi_y^2)}{R'^2_1} \right\} \right] \quad G, \qquad (52)$$

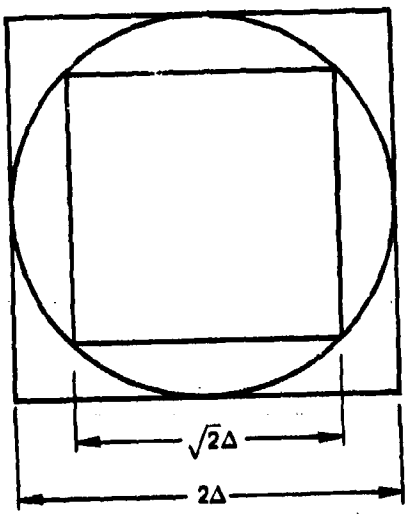

Figure 12. Integration upper and lower bonds in closed form.

where

$$G = \left\{ \frac{1}{2} \operatorname{erf} \left[\Delta - \left(1 - \frac{n}{n'}\right) \bar{R}_x - \frac{(x_0 - x)\theta'_m}{\sqrt{(x - x_0)^2 + (y - y_0)^2}} \right] \frac{1}{U'_\phi} \right.$$

$$\left. - \frac{1}{2} \operatorname{erf} \left[-\Delta - \left(1 - \frac{n}{n'}\right) \bar{R}_x - \frac{(x_0 - x)\theta'_m}{\sqrt{(x - x_0)^2 + (y - y_0)^2}} \right] \frac{1}{U'_\phi} \right\} \cdot$$

$$\left\{ \frac{1}{2} \operatorname{erf} \left[\Delta - \left(1 \frac{n}{n'}\right) \bar{R}_y + \frac{(y_0 - y)\theta'_m}{\sqrt{(x - x_0)^2 + (y - y_0)^2}} \right] \frac{1}{U'_\phi} \right.$$

$$\left. - \frac{1}{2} \operatorname{erf} \left[-\Delta - \left(1 - \frac{n}{n'}\right) \bar{R}_y + \frac{(y_0 - y)\theta'_m}{\sqrt{(x - x_0)^2 + (y - y_0)^2}} \right] \frac{1}{U'_\phi} \right\} . \qquad (53)$$

For small fields of view, G can be replaced by

$$G = \frac{\Omega}{\pi U'^2_\phi} \exp - \frac{1}{U'^2_\phi} \left\{ \left(- \left(1 - \frac{n}{n'}\right) \bar{R}_x - \frac{(x_0 - x)\theta'_m}{\sqrt{(x_0 - x)^2 + (y_0 - y)^2}} \right)^2 \right.$$

$$\left. + \left(- \left(1 - \frac{n}{n'}\right) \bar{R}_y + \frac{(y_0 - y)\theta'_m}{\sqrt{(x_0 - x)^2 + (y_0 - y)^2}} \right)^2 \right\} ; \Omega < U'^2_\phi . \qquad (54)$$

On a final note, it is possible to obtain an estimate of the pulse spreading by referring to figure 13 for the zenith geometry. If the primary contributions come from the disc with diameter z, then the maximum path difference is

$$\rho = \frac{z}{2}(\sec\theta - 1) \; ; \sec\theta = 1.115$$

and the maximum time difference is

$$\Delta t = \frac{n'}{c}\rho = \frac{1.33z}{2c}\,[.115] = 3 \times 10^{-10} z \,. \tag{55}$$

At z = 300 m, ΔT = 90 ns. If the primary contributions come from twice the disk diameter, ΔT = 324 ns.

Heggestad has computed the impulse response of the medium from which he evaluates the delay spread as the 1/e point. This value takes the form

$$\Delta t = \frac{1}{\alpha c}\left[1 + 2\left(\frac{s}{\alpha} - \sqrt{\frac{s}{\alpha}}\right)\alpha z + 2\sqrt{(\alpha z)^2\left(\sqrt{\frac{s}{\alpha}} - 1\right)^2 + \alpha z\left(2\frac{s}{\alpha} - \sqrt{\frac{s}{\alpha}}\right)}\right]. \tag{56}$$

For z = 300 m, this yields 193 ns.

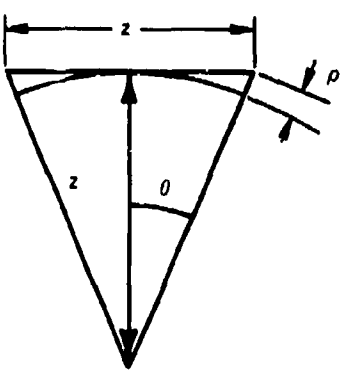

Figure 13. Zenith geometry for estimating pulse spreading.

SUBSURFACE TO SATELLITE BUDGETS

The part of the system most difficult to model has been the subsurface to satellite uplink. This difficulty can best be understood by showing why the two are not reciprocal. On the downlink a 1-mile spot projected from 22000 miles represents an antenna gain of

$$\frac{4\pi\,(22000)^2}{1} \rightarrow 96\ \text{dB}.$$

On the uplink, however, if we go through one scattering length of water, the beam solid angle will be approximately $\overline{\theta^2}$ or an antenna gain of $4\pi/\overline{\theta^2}$. Since $\overline{\theta^2} \sim 10^{-2} - 10^{-1}$, the gain is only 21–31 dB. The gain then goes down as $-10 \log N_{scatt}$ in scattering lengths. Because of the paucity in gain it would be necessary to operate the system closer to the surface on the uplink than for the downlink, if the scattered radiation as described by the Heggestad-Arnush approximation is used exclusively.

For this portion of the link it is necessary to investigate the radiation in greater detail. To do so it is helpful to use the normalized version of the Mutual Coherence Function[11-13] (spatial covariance function). For the scattering function described in equation (3) this becomes

$$\gamma(\rho) = \exp\left[\frac{-\pi^2 r_o^2 \rho^2}{Z^2\lambda^2} + sZ\left\{\frac{1}{\sqrt{1 + (k_o\rho)^2\overline{\theta^2}}} - 1\right\}\right]. \tag{57}$$

Notice that at $\rho = 0$ this is normalized to unity, and we assumed a gaussian source with an aperture equal to πr_o^2 focused at infinity. In normal system design we are commonly interested in the beamwidth of the antenna defined at the 3 dB points. Since the Mutual Coherence Function (MCF) is the transform of the angular distribution of the source as seen by the receiver, we can equivalently define a 'coherence length' ρ_c as a comparable measure of antenna collimation. Thus, the greater the coherence length, the closer the source appears to approximate an impulse in angle (point source). By setting the MCF equal to $e^{-.693}$(-3dB) and solving for ρ_c, we can investigate the behavior or the radiation as it traverses the scattering medium. The expression for ρ_c becomes

$$\rho_c = 1.864\left(\frac{\lambda Z}{\pi r_o}\right) : Z \leq \frac{.693}{s}$$

$$\rho_c = \lambda\frac{\left[\left\{1.386(sZ) - .48\right\}/\overline{\theta^2}\right]^{1/2}}{2\pi|sZ - .693|} : Z > \frac{.693}{s} \tag{58}$$

which is shown in figure 14 as a function of Z for an initial divergence of 10^{-3} radians, and for the water properties defined by s = 0.6, a = .04 and $\overline{\theta^2}$ = .01. Notice that for a distance Z = .693/s the beam propagates as it would in vacuum, and the correlation length increases as the beam diverges. However, the scattering mechanisms abruptly take hold at this distance and the coherence length decreases dramatically in a very short distance, and rapidly

[11] Wells, W. H., "Loss of Resolution in Water as a Result of Multiple Small-Angle Scattering," JOSA, vol 59, no 6, 1969, p 1109

[12] Lutomirski, R. F., private communication

[13] Livingston, P. M., private communication

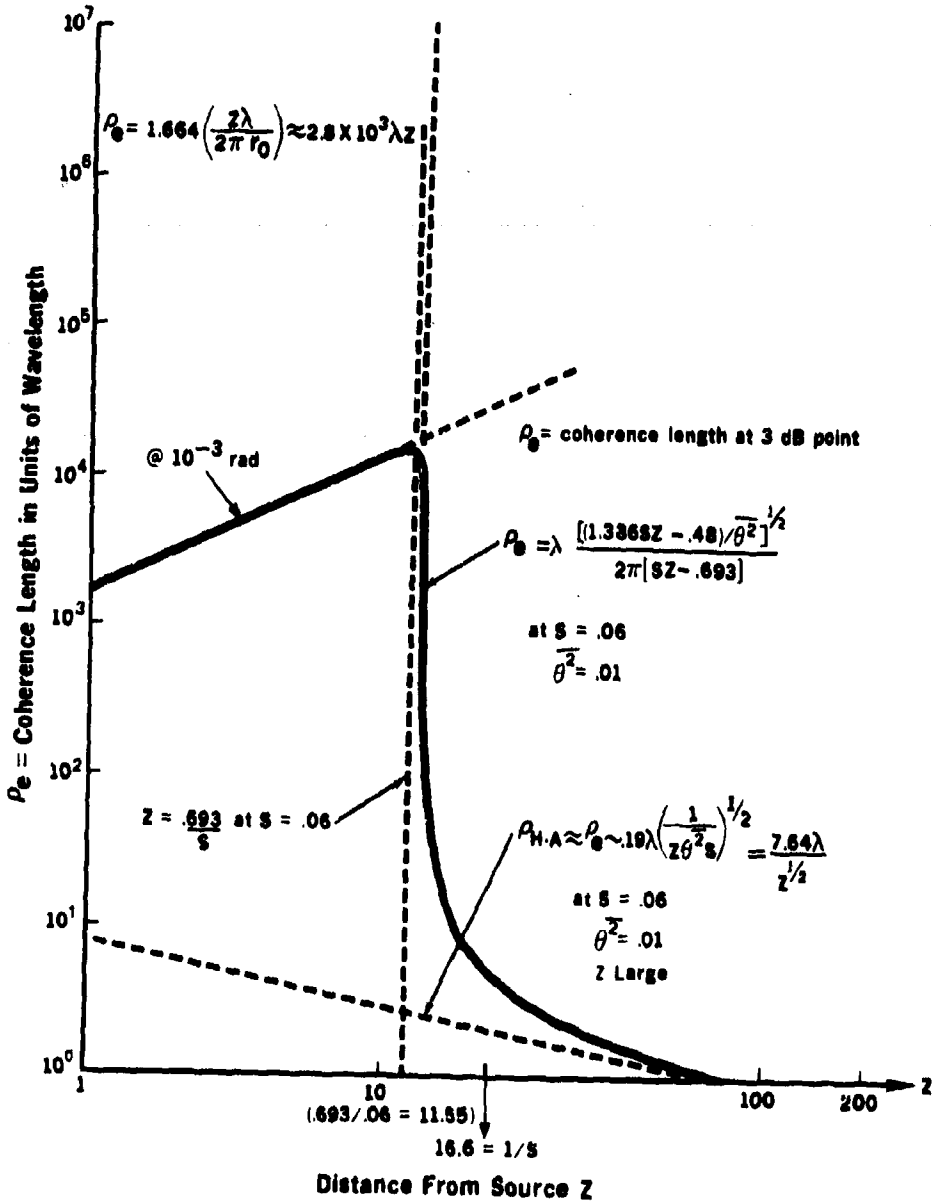

Figure 14. Coherence length as a function of propagation path.

approaches the value

$$\rho_c \approx .19\lambda \left(\frac{1}{s\theta^2 Z}\right)^{1/2} \tag{59}$$

defining the Heggestad-Arnush approximation. Since this behavior is dependent upon the scattering properties of the water, it is instructive to define the albedo[2] ω as the ratio s/(s+a) and the extinction length as N = αZ = (a+s)Z and replot figure 14 for various water parameters in figure 15. Thus we see that we rapidly lose the gain (or imaging capability) of the medium as we traverse a few scattering lengths, which can vary in terms of the extinction length. This, however, is not the whole story.

If we observe the MCF, equation (57), for large values of ρ, we observe the asymptotic value of e^{-sZ}. From Fourier transform theory we know that this corresponds to a point source which relates to the unscattered portion of the beam. And, while the power associated with this portion of the beam is significantly less than that associated with the scattered radiation (lower by e^{-sZ}), it nevertheless retains the full gain of the original source. Consequently, it can be shown that for the uplink geometry a receiver located out of the scattering media at a great distance from the source will always collect more power from this unscattered component than from the scattered component.[12] It is therefore possible to consider the uplink radiation as composed of two additive Gaussian terms – the first retaining all the geometric properties of the radiated source but attenuated by the factor $e^{-(a+s)Z}$, and the second consisting of the scattered portion of the radiation as considered for the downlink. Either of these terms may be used to develop a system, but the resulting systems will have vastly differing operating scenarios due to the difference in coverage and pointing requirements. Consequently, we will consider the general problem of a Gaussian beam propagating up through the air/sea interface and determine the effects.

We will first make the computations outlined in equation (36) for the Heggestad-Arnush approximation and then show how the unscattered result follows. (This component is actually diminished by the factor $1 - \exp\left[-\sqrt{z^2 + (x-x_0)^2 + (y-y_0)^2}\right]$ which we will ignore.)

To compute the surface irradiance profile upon passing through the interface on the uplink it is only necessary to insert equation (7) into equation (36). This yields

$$f(\underline{\gamma}', \underline{r}) = \int d\underline{\gamma}\, p(\underline{\gamma}'/\underline{\gamma})\, f(\underline{\gamma}, \underline{r}) \tag{60}$$

(we assume a collimated, zero cross section source (ℓ=V=0)). Finally, to determine the angular distribution of the beam, $f(\gamma', r)$ is integrated over the surface to yield

$$f(\underline{\gamma}') = \int f(\underline{\gamma}', \underline{r})\, d\underline{r} = \int f(\underline{\gamma}, \underline{r})\, p(\underline{\gamma}'/\underline{\gamma})\, d\underline{\gamma} d\underline{r}. \tag{61}$$

To perform the integration in equation (60), several factors must be taken into account. First recall that we have defined the medium containing the source to have the index n and zenith angle γ. Thus, if we want a more figurative description, we should turn the coordinate system in figure 9 upside down to yield figure 16.

Next recall that we projected the true slope statistics of the surface onto the x and y coordinates. However, the scattered beam has circular symmetry with regard to the angular divergence. Consequently, it is again necessary to rotate the axis of the angular coordinates by the transformation in equation (47), which will allow us to perform the integration in

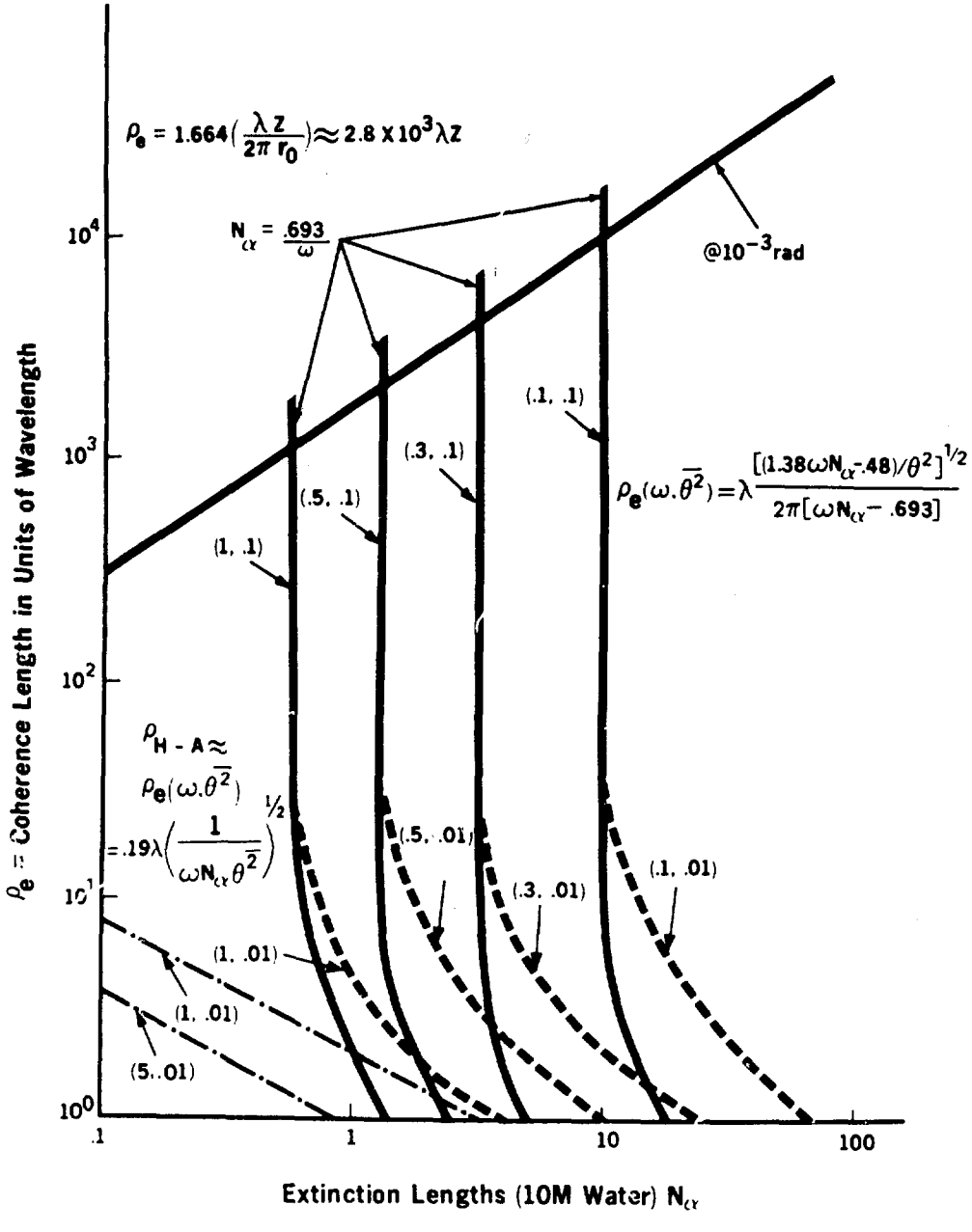

Figure 15. Coherence length as a function of extinction lengths for various values of the albedo and $\overline{\theta^2}$.

equation (60) in Cartesian coordinates. Taking the latter remarks into account and again assuming Gaussian slope statistics, we obtain the function $f(\underline{\gamma}', \underline{r})$ with

$$f(\underline{\gamma}', \underline{r}) = p_t \int \frac{d\theta_x d\theta_y}{[\pi U_\phi' R_1']^2 \left[2\pi \left| 1 \frac{n}{n'} \right|^2 \text{var}\,[R]\right]} \exp -\Bigg\{ a\sqrt{z^2 + x^2 + y^2}$$

$$+ \frac{\xi_x^2 + \xi_y^2}{R_1'^2} + \frac{1}{U_\phi'^2} \left[\left(\theta_x - \bar{\gamma}_x + \frac{x\theta_m'}{\sqrt{x^2 + y^2}} \right)^2 + \left(\theta_y - \frac{y\theta_m'}{\sqrt{x^2 + y^2}} \right)^2 \right]$$

$$+ \frac{1}{2\left[1 - \frac{n}{n'}\right]^2 \text{var}\,[R]} \left[\left(\gamma_x' - \frac{n}{n'} \theta_x - \left(1 - \frac{n}{n'}\right) R_x \right)^2 \right.$$

$$\left. + \left(\gamma_y' - \frac{n}{n'} \theta_y - \left(1 - \frac{n}{n'}\right) R_y \right)^2 \right] \Bigg\} \quad , \tag{62}$$

where we have assumed that the source is located at $(x_0 = 0, y_0 = 0, z)$ and the surface irradiance profile is over (x, y, z). Consequently, the angular distribution of the emerging beam is obtained by integrating $f(\underline{\gamma}', \underline{r})$ over the variables (x, y).

As the surface roughness goes to zero in equation (62), $p(\underline{\gamma}'/\underline{\gamma})$ approaches the delta function $\delta(\underline{\gamma}' - \underline{\gamma})$. For this case the integration can be performed over θ_x, θ_y to yield

$$f(\underline{\gamma}', \underline{r}) = \frac{P_t}{\left(\pi \frac{n}{n'} U_\phi' R_1'\right)^2} \exp -\Bigg\{ a\sqrt{z^2 + x^2 + y^2} + \frac{\xi_x^2 + \xi_y^2}{R_1'^2}$$

$$+ \frac{1}{\left(\frac{n}{n'}\right)^2 U_\phi'^2} \left[\left(\gamma_x' - \frac{n}{n'} \bar{\gamma}_x + \frac{n}{n'} \frac{x\theta_m'}{\sqrt{x^2 + y^2}} \right)^2 + \left(\gamma_y' - \frac{n}{n'} \frac{y\theta_m'}{\sqrt{x^2 + y^2}} \right)^2 \right] \Bigg\} \tag{63}$$

We can also perform the integration in equation (62) for the narrow-beam case. For this case we can extend the integration from $-\infty$ to ∞, yielding

$$f(\underline{\gamma}', \underline{r}) = \left\{ \frac{1}{U_\phi' \Sigma} \exp -\left[\Delta + \frac{\Gamma}{\Sigma} \right] \right\} \frac{p_t}{\pi R_1'^2} \exp -\Bigg[a\sqrt{z^2 + x^2 + y^2}$$

$$+ \frac{\xi_x^2 + \xi_y^2}{R_1'^2} \Bigg] \quad . \tag{64}$$

where

$$\Sigma = \frac{1}{U'^2_\phi} + \frac{1}{2\left[\frac{n'}{n} - 1\right]^2 \text{var}\,[R]}\,,$$

$$\Delta = \frac{1}{2\left[\frac{n'}{n} - 1\right]^2 \text{var}\,[R]} \left[\left\{\frac{n'}{n}\gamma'_x - \left(\frac{n'}{n} - 1\right) R_x\right\}^2 + \left\{\frac{n'}{n}\gamma'_y - \left(\frac{n'}{n} - 1\right) R_y\right\}^2\right]$$

$$+ \frac{1}{U'^2_\phi}\left[\left\{\bar{\gamma}_x + \frac{x\theta'_m}{\sqrt{x^2+y^2}}\right\}^2 + \left\{\frac{y\theta'_m}{\sqrt{x^2+y^2}}\right\}^2\right] \quad \text{, and}$$

$$\Gamma = \left[\frac{\left\{\bar{\gamma}_x + \frac{x\theta'_m}{\sqrt{x^2+y^2}}\right\}}{U'^2_\phi} + \frac{\left\{\frac{n'}{n}\gamma'_x - \left(\frac{n'}{n} - 1\right) R_x\right\}}{2\left(\frac{n'}{n} - 1\right)^2 \text{var}\,[R]}\right]^2$$

$$+ \left[\frac{\left\{\frac{-y\theta'_m}{\sqrt{x^2+y^2}}\right\}}{U'^2_\phi} + \frac{\left\{\frac{n'}{n}\gamma'_y - \left(\frac{n'}{n} - 1\right) R_y\right\}}{2\left(\frac{n'}{n} - 1\right)^2 \text{var}\,[R]}\right]^2 . \qquad (65)$$

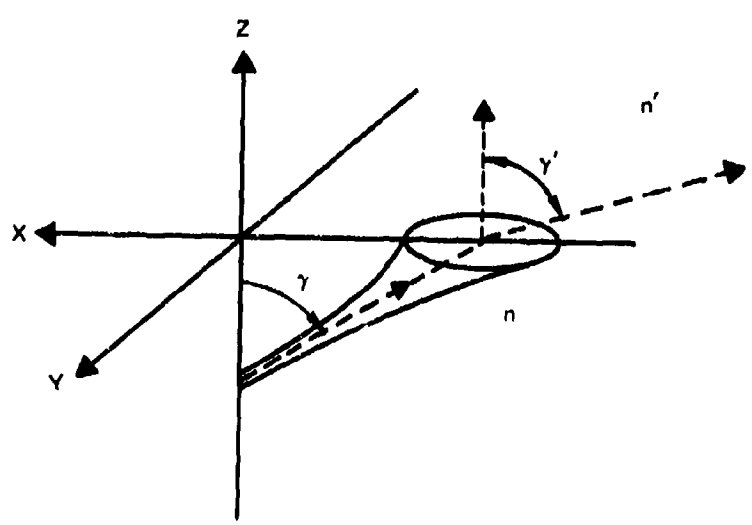

Figure 16. Coordinate system of figure 9 turned upside down.

For the case in which the ocean roughness is absent, equation (60), we see that the exiting beam is centered around the linearized Snell's angle, $(n/n')\overline{\gamma}_x$, but somewhat steered toward the zenith. Physically, this is due to the fact that the scattered paths which lie closest to the zenith traverse a shorter distance and consequently are absorbed less, which skews the beam.

We can integrate the contribution at an angle $\underline{\gamma}'$ over the entire surface as indicated in equation (58). This results in the function $f(\underline{\gamma}')$, which is the angular power distribution. To compute an uplink budget, one needs to integrate $f(\underline{\gamma}')$ over the solid angle subtended by the collecting aperture. At a distance R large enough for the function $f(\underline{\gamma}')$ to be constant over the collecting aperture, this solid angle is merely $A/4\pi R^2$. Consequently, the collected power is

$$p_r = f(\underline{\gamma}') \frac{A}{4\pi R^2} \quad . \tag{66}$$

An important case to notice is when the beam is exiting the water at the zenith and the surface is smooth. Then equation (63) integrated over the hemisphere yields the result in equation (49), multiplied by the normalized angular distribution

$$\frac{1}{\pi\left(\frac{n}{n'} U'_\phi\right)^2} e^{-\frac{\left(\gamma'^2_x + \gamma'^2_y\right)}{\left(\frac{n}{n'} U'_\phi\right)^2}} \quad . \tag{67}$$

If we look at the 3-dB contour, the beam half angle is $(n/n')U'_\phi \sqrt{0.693}$, and the effective gain is

$$G = \frac{2}{1 - \cos\left(\frac{n}{n'} U'_\phi \sqrt{0.693}\right)} \quad . \tag{68}$$

The link loss for this case becomes $(\gamma'_x = \gamma'_y = 0)L$, where

$$L = \frac{f(\underline{\gamma}')|_{\gamma' = 0}}{p_t} = \frac{A}{\pi\left(\frac{n}{n'} U_\phi\right)^2 (4\pi R^2)} \int_{-\infty}^{\infty} \int \frac{1}{\pi R'^2_1 \left(\frac{U'_\phi}{U_\phi}\right)^2}$$

$$\exp - \left\{ a\left[z^2 + x^2 + y^2\right]^{1/2} + \frac{\xi_x^2 + \xi_y^2}{R'^2_1} \right\}_{x_0 = y_0 = \overline{\gamma}_x = 0} dxdy \quad . \tag{69}$$

To obtain the results for the unscattered beam, we would use equation (6) in place of equation (7). This, however, merely requires the substitutions

$$
\begin{aligned}
&S = 0 \\
&R'^2_o \to r_o^2 \\
&U'^2_r \to \theta_o^2 \\
&U'^2_\phi \to \theta_o^2 \\
&R'^2_1 \to r_o^2 + \theta_o^2 Z'^2 \approx \theta_o^2 Z'^2 \\
&P'_t \to P_t e^{-sZ'};\ Z' = \sqrt{z^2 + x^2 + y^2}
\end{aligned}
\tag{70}
$$

with $\theta_m = r_m = 0$. With these substitutions, equations (62, 63, 64, 67, 68, 69) become equations (71 – 76), respectively:

$$
\begin{aligned}
f(\gamma', r) = P_t \int \frac{d\theta_x d\theta_y}{[\pi Z'^2 \theta_o^2]^2 2\pi \left|1 - \frac{n}{n'}\right|^2 \text{var}\,[R]} \exp - \Bigg\{ & \alpha \sqrt{z^2 + x^2 + y^2} \\
& + \frac{\xi_x^2 + \xi_y^2}{\theta_o^2 (z^2 + x^2 + y^2)} + \frac{1}{\theta_o^2} \left[(\theta_x - \bar{\gamma}_x)^2 + \theta_y^2\right] \\
& + \frac{1}{2\left[1 - \frac{n}{n'}\right]^2 \text{var}\,[R]} \left[\left(\gamma'_x - \frac{n}{n'}\theta_x - \left(1 - \frac{n}{n'}\right) R_x\right)^2 + \left(\gamma'_y - \frac{n}{n'}\theta_y - \left(1 - \frac{n}{n'}\right) R_y\right)^2\right] \Bigg\}
\end{aligned}
\tag{71}
$$

$$
\begin{aligned}
f(\gamma', r) = \frac{P_t}{\left(\pi \frac{n}{n'} Z' \theta_o^2\right)^2} \exp - \Bigg\{ & \alpha \sqrt{z^2 + x^2 + y^2} + \frac{\xi_x^2 + \xi_y^2}{\theta_o^2 Z'^2} \\
& + \frac{1}{\left(\frac{n}{n'}\right)^2 \left(\theta_o^2\right)} \left[\left(\gamma'_x - \frac{n}{n'}\bar{\gamma}_x\right)^2 + \gamma'^2_y\right] \Bigg\}
\end{aligned}
\tag{72}
$$

$$
f(\underline{\gamma}', \underline{r}) = \frac{1}{\theta_o^2 \Sigma} \exp - \left[\Delta + \frac{\Gamma}{\Sigma}\right] \frac{P_t}{\theta_o^2 Z'^2} \exp - \left[\alpha \sqrt{x^2 + y^2 + z^2} + \frac{\xi_x^2 + \xi_y^2}{\theta_o^2 Z'^2}\right] \tag{73}
$$

$$\frac{1}{\pi\left(\frac{n}{n'}\right)^2\left(\theta_o^2\right)} \exp - \frac{\gamma_x'^2 + \gamma_y'^2}{\left(\frac{n}{n'}\right)^2\left(\theta_o^2\right)} \tag{74}$$

$$G' = \frac{2}{1 - \cos\left(\frac{n}{n'}\sqrt{\theta_o^2\,(.693)}\right)} \tag{75}$$

$$L' = \frac{A}{\pi\left(\frac{n}{n'}\right)^2 \theta_o^2 \,(4\pi R^2)} \iint_{-\infty}^{\infty} \frac{dxdy}{\pi\theta_\delta^2 Z'^2}$$

$$\exp - \left\{ \alpha\sqrt{z^2 + x^2 + y^2} + \frac{\xi_x^2 + \xi_y^2}{\theta_o^2 Z'^2}\Bigg|_{x_o = y_o = \bar{\gamma}_x = 0} \right\} . \tag{76}$$

We again point out that for large zenith angles, the linearization used to derive these results is not valid, and a more detailed analysis is required.

Comparing equations (68) and (75) and letting $\cos X = 1 - \frac{X^2}{2}$, we see that the ratio of the gain in the unscattered to scattered beam on axis is

$$\frac{N_s\theta^2}{(\lambda/r_o)^2} . \tag{77}$$

where we have assumed that the beam is focused at infinity ($\theta_o = \lambda/r_o$) and we are transmitting from N_s scattering lengths. Since the unscattered beam has e^{-N_s} times the power of the scattered beam, we see that the inequality

$$\frac{N_s\theta^2 e^{-N_s}}{(\lambda/r_o)^2} \leq 1 \tag{78}$$

determines which portion dominates.

DISCUSSION

In this document we have developed models for use in evaluating the performance of the duplex subsurface to above-surface optical communications systems. We will now briefly discuss the limitations of the models and the areas of applicability. We will also point out relevant areas of future work. The first aspect of the model is the estimate of underwater propagation. The Heggestad-Arnush model used appears to have all the attributes necessary for accurate predictions. Although the model has been calibrated to existing data, an independent verification is warranted. The results of such an effort would determine whether or not further refinement is necessary. The major implication of this propagation model is a clear distinction between the contributions of absorption and scattering to the extinction coefficient. Couched in system terminology, the model states that if the size of the beam on the surface is comparable to or greater than the depth from which it is to be viewed, and if the field of view at the receiver can be made large, then the only loss is from absorption. Since the extinction coefficient is usually two or more times greater than the absorption coefficient, the depth prediction under these conditions would also be two or more times greater than predicted from the extinction coefficient alone. The field of view encountered is also seen to be proportional to the square root of the scattering coefficient and the depth.

The second aspect of the model relates to the effects of the surface. In order to obtain usable results, a linearization of Snell's law was employed which should be reasonably accurate for zenith angles out to 45°. The important result is that at sufficient depth the effects of a random surface would be negligible. The major concern should be blockage of light due to foam, etc. The basis of this conclusion stems from the prediction that the rms beam spreading will be proportional to $|1 - (n/n'|$ times the rms slope distribution of the surface. This would imply that a maximum of 5° or so is all that would ever be expected. The major impact would seem to be on the uplink, where beam steering would occur.

The most difficult part of this communication system appears to be the uplink. Because of the nonreciprocal nature of the duplex system, the unscattered portion of the beam provides the greater potential for power transfer. However, the power in this portion of the beam is greatly diminished over the scattered term, yet retains its high directionality. The diminished power implies a depth reduction of $a/(a+s)$. In addition the spot size on the ocean surface will not encompass enough area to average out the dynamic effects of the wave motion. Consequently, measures will have to be taken to compensate for this wave motion in an active and dynamic manner This implies a form of image inhancement of the downlink beam so as to track the unscattered component. This is an area where future work can be directed and efforts are already underway.

REFERENCES

1. Kennedy, R. S., "Communication through Optical Scatte ing Channels: An Introduction," Proc IEEE, vol 58, no 10, p 1651-65, 1970

2. Lerner, R. M., and Holland, A. E., "The Optical Scatter Channel," Proc IEEE, vol 58, no 10, p. 1547-1563 1970

3. Bucher, E. A., Lerner, R. M., and Niessen, C. W., "Some Experiments on the Propagation of Light Pulses through Clouds," Proc IEEE, vol 58, no 10, p 1564-67, 1970

4. Heggestad, H. M., "Optical Communication through Multiple Scattering Media," MIT/RLE Technical Report 472, November 1968

5. Arnush, D., "Underwater Light-Beam Propagation in the Small-Angle Scattering Approximation," JOSA, 62, p 1109-1111, 1972

6. Jerlov, N. G., "Optical Oceanography," Elsevier, 1968

7. Duntley, S. Q., "Underwater Lighting by Submerged Lasers," Visibility Laboratory, SIO ref 71-1, June 1971

8. Swennen, J. P. J. W., "Time-Average Power-Density Probability Distribution below the Ocean Surface of a Beam of Collimated Optical Radiation Incident on the Surface," JOSE 56, p 224-229, 1966

9. Stratton, J. A., "Electromagnetic Theory," McGraw Hill, 1941

10. Cox, C., and Munk, W., Bulletin Scripps Inst Oceanog Univ California 6 401, 1956

11. Wells, W. H., "Loss of Resolution in Water as a Result of Multiple Small-Angle Scattering," JOSA, vol 59, no 6, June 1969, p 1109